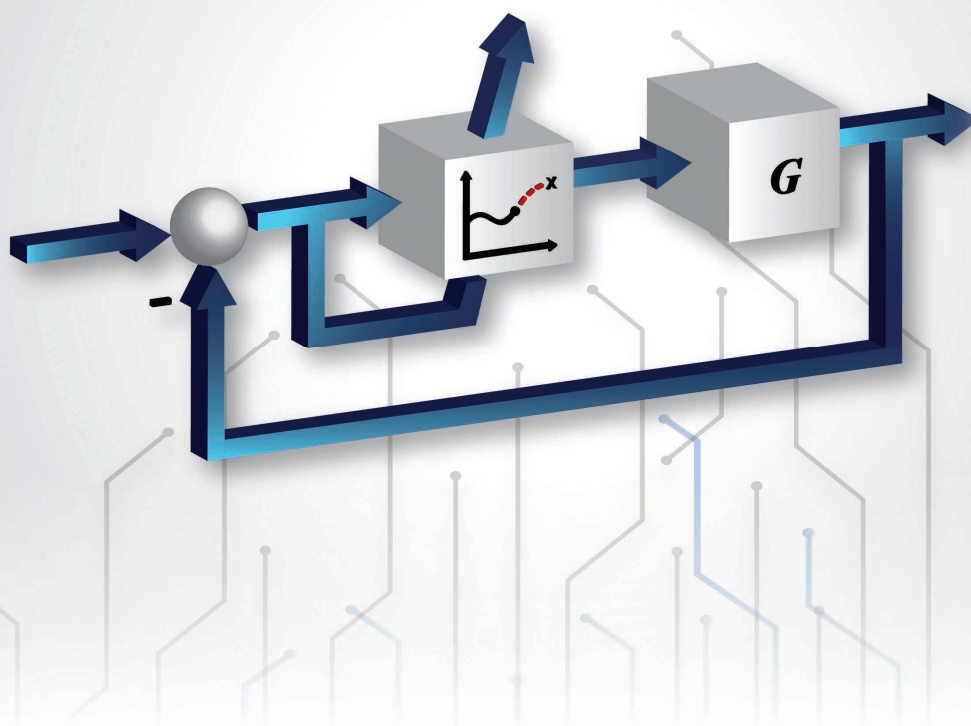


# Predictive Cost Adaptive Control

## A NUMERICAL INVESTIGATION OF PERSISTENCY, CONSISTENCY, AND EXIGENCY



ZARNEEN AZMAT

TAM W. NGUYEN, SYED ASEEM UL ISLAM,  
DENNIS S. BERNSTEIN, and ILYA V. KOLMANOVSKY

**A**mong the multitude of modern control methods, model predictive control (MPC) is one of the most successful [1]–[4]. As noted in “Summary,” this success is largely due to the ability of MPC to respect constraints on controls and enforce constraints on outputs, both of which are difficult to handle with linear control methods, such as linear quadratic regulator

(LQR) and linear quadratic Gaussian (LQG), and nonlinear control methods, such as feedback linearization and sliding mode control. Although MPC is computationally intensive, it is more broadly applicable than Hamilton–Jacobi–Bellman-based control and more suitable for feedback control than the minimum principle. In many cases, the constrained optimization problem for receding-horizon optimization is convex, which facilitates computational efficiency [5].

MPC uses a model of the plant with constrained receding-horizon optimization to compute a sequence of

Digital Object Identifier 10.1109/MCS.2021.3107647  
Date of current version: 12 November 2021

future control inputs. The first element of the optimized sequence is implemented, and the remaining elements are discarded. At a first glance, this strategy seems ad hoc and wasteful. However, receding-horizon optimization is known to be asymptotically stabilizing for a sufficiently long prediction horizon or with terminal constraints, and, if the initial state is feasible and the model matches the plant, it is recursively feasible with respect to constraints [6]–[9].

MPC handles convex control and output constraints efficiently compared to conventional feedback control methods that treat control constraints as input nonlinearities. In particular, linear dynamics with control magnitude and move-size (rate) saturation comprise a Hammerstein system [10]–[12], whose importance is reflected by the vast literature on bounded control and antiwindup strategies [13]–[15]. Within the context of MPC, however, magnitude and move-size control constraints are treated as optimization constraints rather than explicit nonlinearities, which simplifies the treatment of this problem.

From the perspective of classical control and modern optimal state-space control, MPC is a paradigm shift. For example, conventional feedback methods use integral action to asymptotically follow step commands and reject step disturbances, and it is common practice to embed integrators within LQR and LQG controllers. MPC, however, performs numerical optimization at each step, and thus no integrator per se appears [8]. Without integral action, MPC lacks one of the key strengths of classical control, namely, the ability to follow setpoint commands and reject step disturbances without knowledge of the dc gain of the plant. On the other hand, by eschewing integral action, MPC is not degraded by integrator windup.

Since MPC uses model-based prediction to determine future control inputs, it follows that these predictions require knowledge of future commands and disturbances. Future commands are sometimes known; this is the aim of preview control and trajectory-tracking methods [16], [17]. On the other hand, except for disturbance-feedforward control architectures [18], disturbances are rarely known, especially in the future. The lack of future knowledge of commands and disturbances thus represents a potential obstacle for MPC.

Although MPC is often based on linear models, this technique is also applicable to nonlinear systems [19]. An additional challenge is the case of output feedback, where not all of the plant states are measured. In this case, state estimation can be used to provide estimates of unmeasured states, where the state estimates serve as ersatz states for the receding-horizon optimization [20]–[24]. Transient errors in the state estimates, however, can impede the ability to enforce constraints on unmeasured states. Output-feedback MPC that does not rely on a state estimator is developed in [25]–[30] and [8, Ch. 5].

In addition to the lack of knowledge about future commands and disturbances, a potential weakness of MPC is the need for a sufficiently accurate model for effective predictive optimization.

## Summary

**M**odel predictive control, which is based on receding-horizon optimization, is a widely used modern control technique with numerous successful application in diverse areas. Much of this success is due to the ability of receding-horizon optimization to enforce state and control constraints, which are crucial in many applications of control. To avoid the need for an observer, predictive cost adaptive control (PCAC) uses the block observable canonical form, whose state consists of past values of the control inputs and measured outputs. PCAC also uses recursive least squares (RLS) with variable-rate forgetting for online identification.

The article describes the algorithmic details of PCAC and numerically investigates its performance through a collection of numerical examples that highlight various control challenges, such as model-order uncertainty, sensor noise, prediction horizon, stabilization, magnitude and move-size saturation, and stabilization. The numerical examples are used to probe the performance of PCAC in terms of persistency, consistency, and exigency. Since, unlike dual control, PCAC does not employ a separate control perturbation to enhance persistency, the focus is on self-generated persistency during transient operation. For closed-loop identification using RLS, sensor noise gives rise to bias in the identified model, and the goal is to determine the effect of the lack of consistency. Finally, the numerical examples are used to assess exigency, which is the extent to which the online identification emphasizes model characteristics that are most relevant to meeting performance objectives.

This dependence is mitigated by robust MPC techniques [31], [32], minimax techniques for minimizing the loss of a worst-case scenario, and robust tube-based MPC [33]–[35].

As an alternative to robust MPC, extensions of MPC to include online identification and learning are considered in [36]–[39]. These techniques can potentially overcome the worst-case considerations of robust MPC by allowing MPC to learn the true plant dynamics and disturbances. For system identification, the commands, disturbances, and control inputs must provide sufficient *persistency* to facilitate identification. Concurrent learning with MPC can be viewed as a form of indirect adaptive control [40]. Within this context, the role of persistency is a longstanding issue [41]. More generally, indirect adaptive control can be viewed as a specialized version of data-driven control [42]–[48].

Beyond persistency, since online identification and learning occur during closed-loop operation, the control input is correlated with the measurements due to disturbances and sensor noise. When recursive least squares (RLS) is used for closed-loop identification, this correlation may obstruct *consistency* and, thus, lead to asymptotic bias in the parameter estimates [49]–[51]. Alternative identification methods, such as the prediction error method (PEM) [52] and instrumental variables (IV) [53],

provide consistency despite signal correlation. Using numerical examples to examine asymptotic bias, RLS, PEM, and IV are applied to open-loop identification, closed-loop identification using a fixed-gain linear controller, and MPC control, where the identified plant model is updated at each step.

Since MPC is an inherently discrete-time control technique, its application to plants with continuous-time dynamics entails a sampled-data plant with analog-to-digital sampling and digital-to-analog input reconstruction. As in any sampled-data controller implementation, the sampling rate must be chosen to minimize aliasing and folding effects [54], [55]. Within this context, MPC provides direct digital control of discretized plants without the need to discretize continuous-time controllers. The present article considers examples with sampled-data dynamics to assess the intersample response [56]–[58].

The present article focuses on MPC for constrained linear plants with two nonstandard features. First, only a limited number of states of the plant are assumed to be measured; this is the case of output feedback rather than full-state feedback. Instead of using an observer to provide estimates of unmeasured states, the present article takes advantage of the block observable canonical form (BOCF) [59], which is a state-space realization whose state is a function of measured inputs and outputs. This realization thus removes the need to build an observer to estimate unmeasured states. Within this framework, a key assumption is the availability of measurements of all constrained outputs.

The second feature of the present article is the use of online identification to construct and refine a model for the constrained receding-horizon optimization. Concurrent identification is performed with RLS [60], [61] with the additional benefit of variable-rate forgetting (VRF) [62], [63].

**TABLE 1** The key takeaways from each example. MIMO: multiple-input, multiple-output; VRF: variable-rate forgetting.

Example	Key Takeaways
1	<ul style="list-style-type: none"> <li>• Robustness to model order</li> <li>• Self-generated persistency</li> <li>• Exigency</li> </ul>
2	<ul style="list-style-type: none"> <li>• Stabilization</li> <li>• Self-generated persistency</li> </ul>
3	<ul style="list-style-type: none"> <li>• Stabilization of unstably stabilizable plants</li> </ul>
4	<ul style="list-style-type: none"> <li>• Harmonic and broadband disturbance rejection</li> <li>• Exigency</li> </ul>
5	<ul style="list-style-type: none"> <li>• Output constraints</li> <li>• Role of relaxation weight</li> </ul>
6	<ul style="list-style-type: none"> <li>• Unmatched broadband disturbance rejection for MIMO plants</li> </ul>
7	<ul style="list-style-type: none"> <li>• Stabilization and output constraints for MIMO plants</li> </ul>
8	<ul style="list-style-type: none"> <li>• Importance of VRF for abruptly changing systems</li> </ul>
9	<ul style="list-style-type: none"> <li>• Tuning VRF in the presence of sensor noise</li> </ul>
10	<ul style="list-style-type: none"> <li>• Enforcement of constraints for abruptly changing systems</li> </ul>

The present article describes predictive cost adaptive control (PCAC), which incorporates the two features described previously. No attempt is made in this article to derive stability or performance guarantees for this approach. Instead, the goal is to systematically investigate PCAC through a collection of numerical examples. These examples are chosen to highlight the stability and performance of PCAC for a diverse collection of plants and scenarios. These scenarios include the effect of model order; sensor noise; unknown step, harmonic, and broadband disturbances; stabilization; sampled-data effects; magnitude and move-size control constraints; output constraints; and abrupt and gradual changes in the plant.

The numerical examples in this article provide a venue for investigating the interplay between identification and control, a longstanding problem in control theory [64]–[66]. This interplay is addressed by dual control, where the objective is to determine probing signals that enhance persistency and, thus, the speed and accuracy of the concurrent identification [67]–[69]. In contrast to dual control, PCAC does not require a separate probing input, such as the dither signal used by extremum-seeking control to estimate gradients [70]. Instead, the present article investigates the phenomenon of *self-generated persistency*, where PCAC automatically increases the persistency of the control signal in response to the closed-loop performance.

Within the context of PCAC, the interplay between identification and control is embodied by *exigency*, which refers to the ability of the identification to prioritize features of the identified model that impact closed-loop performance. A key goal of the numerical examples is, thus, to explore manifestations of persistency, consistency, and exigency within PCAC. This article extends the preliminary investigation of PCAC given in [71] and [72] through refinements of the control algorithm; more extensive numerical examples; and an investigation of persistency, consistency, and exigency. Table 1 lists the key takeaways from each numerical example.

The next section describes the control architecture within which this article is framed. Next, elements of PCAC are described, which include input–output models, the BOCF for an input–output predictive model, and quadratic programming (QP). Linear single-input, single-output (SISO) Examples 1–5 are then presented, followed by linear multiple-input, multiple-output (MIMO) Examples 6 and 7, which are followed by linear time-varying Examples 8–10. Conclusions and directions for future research are then presented.

## NOTATION

The  $n \times n$  identity matrix is denoted by  $I_n$ , the  $m \times n$  matrix of ones by  $1_{m \times n}$ , the  $m \times n$  matrix of zeros by  $0_{m \times n}$ , and the Kronecker product by  $\otimes$ . The infinity norm of a vector  $x = [x_1 \dots x_n]^T \in \mathbb{R}^n$  is defined by  $\|x\|_\infty \triangleq \max(|x_1|, \dots, |x_n|)$ .

## CONTROL ARCHITECTURE AND OBJECTIVES

The examples in this article consider the control architecture shown in Figure 1. In some cases, the continuous-time plant  $G$  is specified as a transfer function or state-space model. In these



» *Receding-horizon optimization:* Using the identified model (8), QP is used to perform receding-horizon optimization to determine the next control input.

### Recursive Least Squares With Variable-Rate Forgetting for Online Identification

For online identification, RLS is used to estimate the coefficients of the input-output model (8). To do this, RLS minimizes the cumulative cost

$$J_k(\hat{\theta}) = \sum_{i=0}^k \frac{\rho_i}{\rho_k} z_i^T(\hat{\theta}) z_i(\hat{\theta}) + \frac{1}{\rho_k} (\hat{\theta} - \theta_0)^T P_0^{-1} (\hat{\theta} - \theta_0), \quad (12)$$

where, for all  $k \geq 0$ ,  $\rho_k \triangleq \prod_{j=0}^k \lambda_j^{-1} \in \mathbb{R}$ ,  $\lambda_k \in (0, 1]$  is the forgetting factor,  $P_0 \in \mathbb{R}^{[\hat{n}p(m+p)+mp] \times [\hat{n}p(m+p)+mp]}$  is positive definite, and  $\theta_0 \in \mathbb{R}^{\hat{n}p(m+p)+mp}$  is the initial estimate of the coefficient vector. The performance variable  $z_k(\hat{\theta}) \in \mathbb{R}^p$  is defined by

$$z_k(\hat{\theta}) \triangleq y_k + \sum_{i=1}^{\hat{n}} \hat{F}_i y_{k-i} - \sum_{i=0}^{\hat{n}} \hat{G}_i u_{k-i}, \quad (13)$$

where the vector  $\hat{\theta} \in \mathbb{R}^{\hat{n}p(m+p)+mp}$  of coefficients to be estimated is defined by

$$\hat{\theta} \triangleq \text{vec}[\hat{F}_1 \dots \hat{F}_{\hat{n}} \hat{G}_0 \dots \hat{G}_{\hat{n}}]. \quad (14)$$

Defining the regressor matrix  $\phi_k \in \mathbb{R}^{p \times [\hat{n}p(m+p)+mp]}$  by

## Open- and Closed-Loop Identification Using the Prediction Error Method and Instrumental Variables

This sidebar compares the accuracy of the prediction error method (PEM) and instrumental variables (IV) with recursive least squares (RLS) in open- and closed-loop frameworks. All of the examples in this sidebar consider the asymptotically stable nonminimum-phase (NMP) plant

$$G(z) = \frac{4(z-1.2)}{z^2 - z + 0.8}, \quad (S1)$$

with matched disturbance  $w_k$ . The output  $y_k$  of (S1) is corrupted by sensor noise  $v_k$ , and the noisy output is used for identification. The input  $u_k$  of (S1) is assumed to be known and is also used for identification.

For RLS, let  $\hat{n} = 2$  and  $P_0 = 1000$ . PEM is implemented using the Matlab function `recursiveBJ` with initial parameter covariance 1000, a second-order identification model, and a zeroth-order noise model. Numerical tests with higher-order noise models yielded less accurate results and, thus, are not

shown. IV is implemented using the Matlab function `iv4` with a second-order identification model.

### Example S1: Open-Loop Identification Using Recursive Least Squares and the Prediction Error Method

Let  $u_k, w_k$ , and  $v_k$  be zero-mean, Gaussian white noise sequences with a standard deviation of one. Figure S1 shows the error of the estimate of each coefficient of (S1) versus the time step. Note that all of the PEM coefficient errors approach zero, which indicates consistency. However, the RLS estimates are biased, which shows that RLS lacks consistency.  $\diamond$

### Example S2: Open-Loop Identification Using Recursive Least Squares and Instrumental Variables

Let  $u_k, w_k$ , and  $v_k$  be as in Example S1. Figure S2 shows the error of the estimate of each coefficient of (S1) versus the time step. Note that all of the IV coefficient errors approach zero,

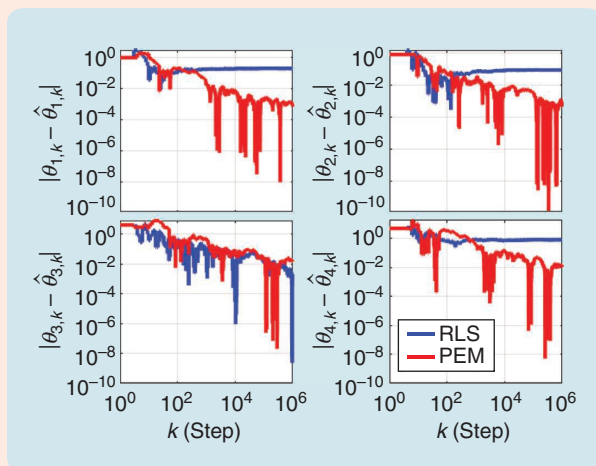


**FIGURE S1** Example S1: Open-loop identification accuracy of the prediction error method (PEM) and recursive least squares (RLS). Note that PEM coefficient errors approach zero.

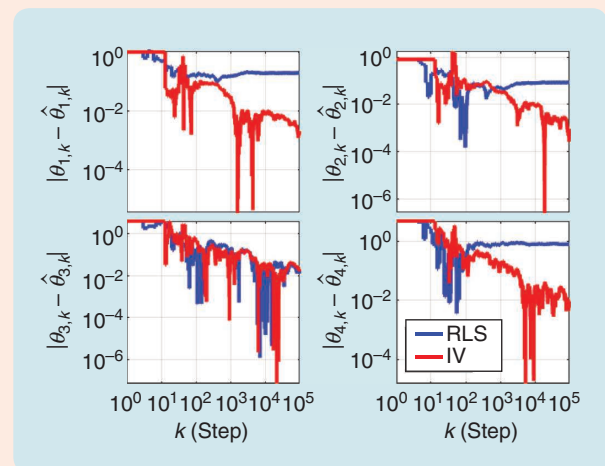


**FIGURE S2** Example S2: Open-loop identification accuracy of recursive least squares (RLS) and instrumental variables (IV). Note that the IV coefficient errors approach zero.

$$\phi_k \triangleq [-y_{k-1}^T \dots -y_{k-\hat{n}}^T \quad u_k^T \dots u_{k-\hat{n}}^T] \otimes I_p, \quad (15)$$

it follows that the performance variable (13) can be rewritten as

$$z_k(\hat{\theta}) = y_k - \phi_k \hat{\theta}. \quad (16)$$

Note that, with (16), the cost function (12) is strictly convex and quadratic and, thus, has a unique global minimizer. The unique global minimizer

$$\theta_{k+1} \triangleq \underset{\hat{\theta}}{\operatorname{argmin}} J_k(\hat{\theta}) = \operatorname{vec}[\hat{F}_{1,k+1} \dots \hat{F}_{\hat{n},k+1} \quad \hat{G}_{0,k+1} \dots \hat{G}_{\hat{n},k+1}] \in \mathbb{R}^{\hat{n}p(m+p)+mp} \quad (17)$$

is computed by RLS as:

### Recursive Least Squares Online Identification

$$L_k = \lambda_k^{-1} P_k, \quad (18)$$

$$P_{k+1} = L_k - L_k \phi_k^T (I_p + \phi_k L_k \phi_k^T)^{-1} \phi_k L_k, \quad (19)$$

$$\theta_{k+1} = \theta_k + P_{k+1} \phi_k^T (y_k - \phi_k \theta_k). \quad (20)$$

Note that  $\theta_{k+1}$  computed using (20) is available at step  $k$ . Thus,  $\hat{F}_{1,k+1}, \dots, \hat{F}_{\hat{n},k+1}, \hat{G}_{0,k+1}, \dots, \hat{G}_{\hat{n},k+1}$  are available at step  $k$ .

The step-dependent parameter  $\lambda_k$  is the *forgetting factor*. In the case where  $\lambda_k$  is constant, RLS uses *constant-rate forgetting (CRF)*; otherwise, RLS uses *VRF* [62]. For VRF,  $\lambda_k$  is given by

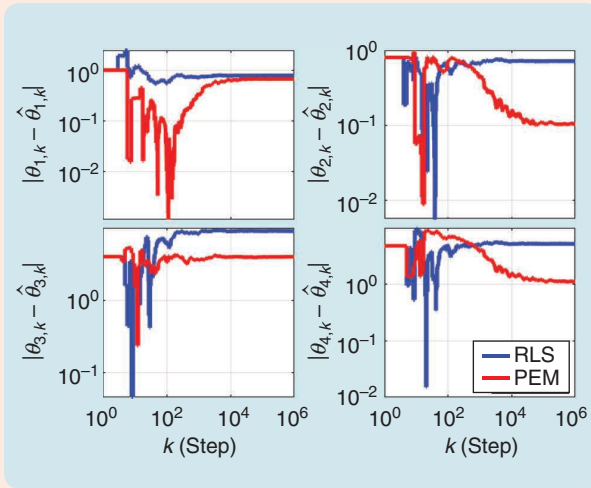


**FIGURE S3** Example S3: Closed-loop identification accuracy of recursive least squares (RLS) and the prediction error method (PEM). Note that the PEM coefficient errors are uniformly smaller than the RLS coefficient errors.

which indicates consistency. However, the RLS estimates are biased, which shows that RLS lacks consistency.  $\diamond$

#### Example S3: Closed-Loop Identification Using Recursive Least Squares and the Prediction Error Method

Let  $w_k$  and  $v_k$  be zero-mean, Gaussian white noise sequences with a standard deviation of 0.1. For closed-loop identification examples, the input  $u_k$  is given by a linear quadratic Gaussian controller designed using the Matlab command `lqg` with weights  $Q_{xu} = Q_{vv} = I_3$ . Figure S3 shows the error of the estimate of each coefficient of (S1) versus the time step. Note that, after convergence, the PEM coefficient errors are uniformly smaller than the RLS coefficient errors; the improvement ranges from 0.71 to 9.05. However, all of the PEM and RLS estimates are biased, which shows that neither method is consistent for this example.  $\diamond$

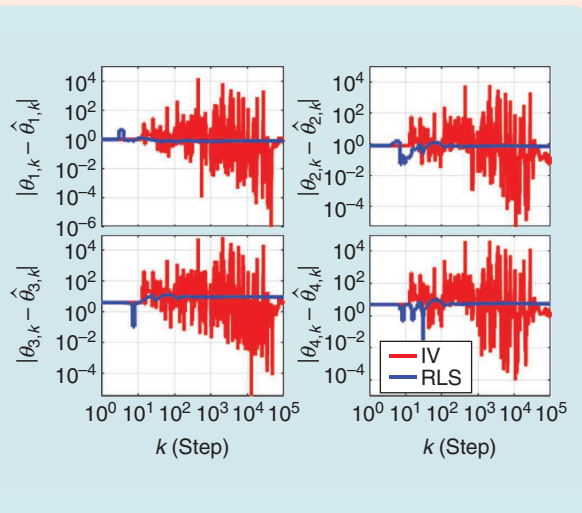


**FIGURE S4** Example S4: Closed-loop identification accuracy of recursive least squares (RLS) and instrumental variables (IV). Note that IV produces large estimation errors.

#### Example S4: Closed-Loop Identification Using Recursive Least Squares and Instrumental Variables

Let  $u_k, w_k$ , and  $v_k$  be as in Example S3. Figure S4 shows the error of the estimate of each coefficient of (S1) versus the time step. Note that the RLS estimates are biased, and IV produces large estimation errors.  $\diamond$

These numerical examples, although limited, demonstrate that PEM is more accurate than RLS for both open-loop and closed-loop identification. Furthermore, although IV showed clear advantages over RLS for open-loop identification, its performance for closed-loop identification is poor, at least for the instruments implemented using the Matlab command `iv4`. Note that these closed-loop identification examples are based on a linear time-invariant controller. The performance of PEM within the context of adaptive control, where the controller is linear time varying, is considered in “Closed-Loop Identification Under Predictive Cost Adaptive Control With the Prediction Error Method.”

$$\lambda_k = \frac{1}{1 + \eta g(z_{k-\tau_d}, \dots, z_k) \mathbf{1}[g(z_{k-\tau_d}, \dots, z_k)]}, \quad (21)$$

where  $\mathbf{1}: \mathbb{R} \rightarrow \{0, 1\}$  is the unit step function, where  $\mathbf{1}(x) = 0$  for all  $x < 0$  and  $\mathbf{1}(x) = 1$  for  $x \geq 0$ , and

$$g(z_{k-\tau_d}, \dots, z_k) \triangleq \frac{\sqrt{\frac{1}{\tau_n} \sum_{i=k-\tau_n}^k z_i^T z_i}}{\sqrt{\frac{1}{\tau_d} \sum_{i=k-\tau_d}^k z_i^T z_i}} - 1. \quad (22)$$

In (21) and (22),  $\eta \geq 0$  and  $0 < \tau_n < \tau_d$  are numerator and denominator window lengths, respectively. Define  $g(0, \dots, 0) \triangleq 0$ . If the sequence  $z_{k-\tau_d}, \dots, z_k$  is zero-mean noise, then the numerator and denominator of (22) approximate the average standard deviation of the noise over the intervals  $[k - \tau_n, k]$  and  $[k - \tau_d, k]$ , respectively. In particular, by choosing  $\tau_d \gg \tau_n$ , it follows that the denominator of (22) approximates the long-term average standard deviation of  $z_k$ , whereas the numera-

tor of (22) approximates the short-term average standard deviation of  $z_k$ . Consequently, the case  $g(z_{k-\tau_d}, \dots, z_k) > 0$  implies that the short-term average standard deviation of  $z_k$  is greater than the long-term average standard deviation of  $z_k$ . The function  $g(z_{k-\tau_d}, \dots, z_k)$  used in VRF suspends forgetting when the short-term average standard deviation of  $z_k$  drops below the long-term average standard deviation of  $z_k$ . This technique prevents forgetting in RLS-based online identification due to zero-mean sensor noise with a constant standard deviation rather than due to the magnitude of the noise-free identification error.

### Receding-Horizon Optimization

Note that (11) can be applied recursively to predict the output over the prediction horizon. A simpler approach that avoids recursion is to use the BOCF state-space realization of (8) given by

## Closed-Loop Identification Under Predictive Cost Adaptive Control With the Prediction Error Method

This sidebar investigates the performance of predictive cost adaptive control (PCAC) when the prediction error method (PEM) is used instead of recursive least squares (RLS). Numerical examples are presented to compare the performance of PCAC/PEM and PCAC/RLS. Note that, unlike the numerical examples considered in “Open- and Closed-Loop Identification Using the Prediction Error Method and Instrumental Variables,” where the controller is linear time invariant, the PCAC controller is adaptive. The examples in this sidebar involve discrete-time plants with matched disturbances  $w_k$ . For each plant, the

output  $y_k$  is corrupted by sensor noise  $v_k$ , and the noisy output is used for identification. The control input  $u_k$ , which is given by receding-horizon optimization, is also used for identification.

For PCAC/PEM, PEM-based identification is combined with receding-horizon optimization. PEM is implemented using the Matlab function `recursiveBJ` with a zeroth-order noise model, model order  $\hat{n}$ , and initial parameter covariance  $P_0$ . Furthermore, the identification model in PEM is initialized at  $\theta_0$ . Both PCAC/PEM and PCAC/RLS use  $u_{\min} = -1, u_{\max} = 1, \Delta u_{\min} = -1, \Delta u_{\max} = 1, \ell = 50, \bar{Q} = 50I_{\ell-1}, \bar{P} = 50, R = 10I_{\ell}$ ,

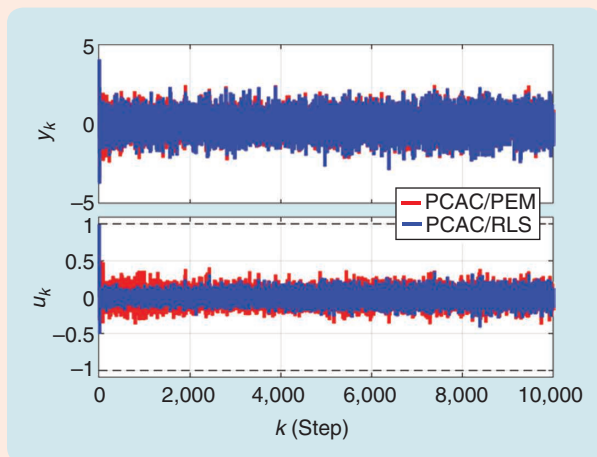


**FIGURE S5** Example S5: Adaptive control of the asymptotically stable plant (S1) using predictive cost adaptive control (PCAC)/prediction error method (PEM) and PCAC/recursive least squares (RLS). PCAC/PEM and PCAC/RLS have 2.03- and 1.70-dB suppression relative to the open-loop response, respectively.

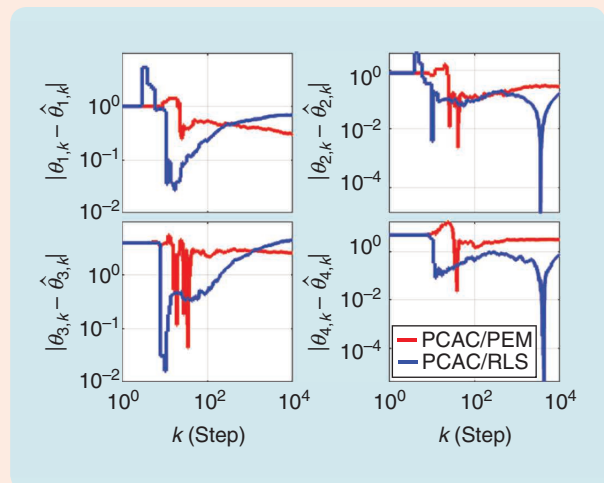


**FIGURE S6** Example S5: Closed-loop identification accuracy of the prediction error method (PEM) and recursive least squares (RLS) operating within predictive cost adaptive control (PCAC)/PEM and PCAC/RLS. Note that neither algorithm is uniformly more accurate.

$$x_{1|k} \triangleq \hat{A}_k \hat{x}_k + \hat{B}_k u_k, \quad (23)$$

$$y_k = C_k \hat{x}_k + \hat{D}_k u_k, \quad (24)$$

where  $x_{1|k} \in \mathbb{R}^{\hat{n}p}$  is the 1-step predicted state,  $\hat{x}_k \triangleq [\hat{x}_{1,k}^T \dots \hat{x}_{\hat{n},k}^T]^T \in \mathbb{R}^{\hat{n}p}$ , and

$$\hat{x}_{1,k} \triangleq y_k - \hat{G}_{0,k+1} u_k, \quad (25)$$

$$\hat{x}_{i,k} \triangleq - \sum_{j=1}^{\hat{n}-i+1} \hat{F}_{i+j-1,k+1} y_{k-j} + \sum_{j=1}^{\hat{n}-i+1} \hat{G}_{i+j-1,k+1} u_{k-j}, \quad i = 2, \dots, \hat{n}, \quad (26)$$

$$\hat{A}_k \triangleq \begin{bmatrix} -\hat{F}_{1,k+1} & I_p & \cdots & \cdots & 0_{p \times p} \\ \vdots & 0_{p \times p} & \ddots & & \vdots \\ \vdots & \vdots & \ddots & \ddots & 0_{p \times p} \\ \vdots & \vdots & & I_p & \\ -\hat{F}_{\hat{n},k+1} & 0_{p \times p} & \cdots & \cdots & 0_{p \times p} \end{bmatrix}, \quad \hat{B}_k \triangleq \begin{bmatrix} \hat{G}_{1,k+1} - \hat{F}_{1,k+1} \hat{G}_{0,k+1} \\ \hat{G}_{2,k+1} - \hat{F}_{2,k+1} \hat{G}_{0,k+1} \\ \vdots \\ \hat{G}_{\hat{n},k+1} - \hat{F}_{\hat{n},k+1} \hat{G}_{0,k+1} \end{bmatrix}, \quad (27)$$

$$C \triangleq [I_p \ 0_{p \times p} \ \cdots \ 0_{p \times p}], \quad \hat{D}_k \triangleq \hat{G}_{0,k+1}. \quad (28)$$

The model structure (8) and its realization (27), (28), which extends the SISO construction given in [59], provides the basis for the output prediction described below. Note that (25) and (26) depend on past values of the measurement  $y_k$  and control  $u_k$  rather than the 1-step predicted output  $y_{1|k}$  given by (9) and 1-step computed input  $u_{1|k}$  given in the next section.

Using (23), the 1-step predicted output given by (9) can be rewritten as

$$y_{1|k} = C x_{1|k} + \hat{D}_k u_{1|k}. \quad (29)$$

Similarly, defining the  $i$ -step predicted state

$$x_{i|k} \triangleq \hat{A}_k x_{i-1|k} + \hat{B}_k u_{i-1|k}, \quad i \geq 2, \quad (30)$$

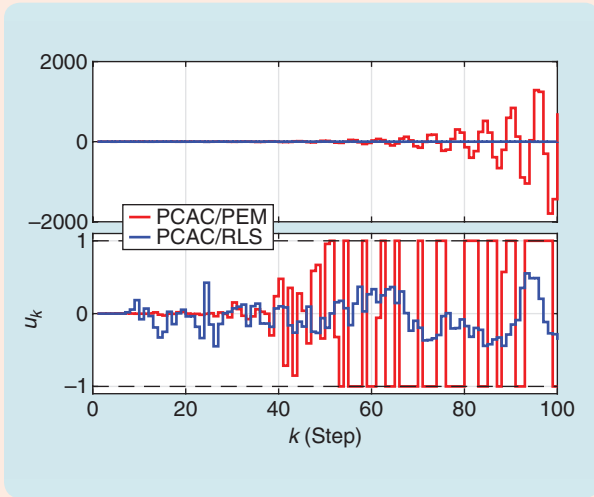


**FIGURE S7** Example S6: Adaptive control of the unstable plant (S2) using predictive cost adaptive control (PCAC)/prediction error method (PEM) and PCAC/recursive least squares (RLS). Note that PCAC/PEM fails to stabilize the plant.

$\lambda = 1$ ,  $\hat{n} = 2$ ,  $\theta_0 = 10^{-2} \cdot 1_{2\hat{n} \times 1}$ ,  $P_0 = 10^3 I_{2\hat{n}}$ , and a strictly proper identification model.

#### Example S5: An Asymptotically Stable Plant

Let  $G(z)$  be given by (S1), and let  $w_k$  and  $v_k$  be as in Example S3. Figure S5 shows  $y_k$  and  $u_k$  for PCAC/PEM and PCAC/RLS. Figure S6 shows the error of each coefficient of (S1) versus the time step obtained with PCAC/PEM and PCAC/RLS. Note that all of the PEM and RLS estimates are biased, which shows that, for this example, neither method is consistent. However, RLS is uniformly faster in reducing the identification errors.  $\diamond$

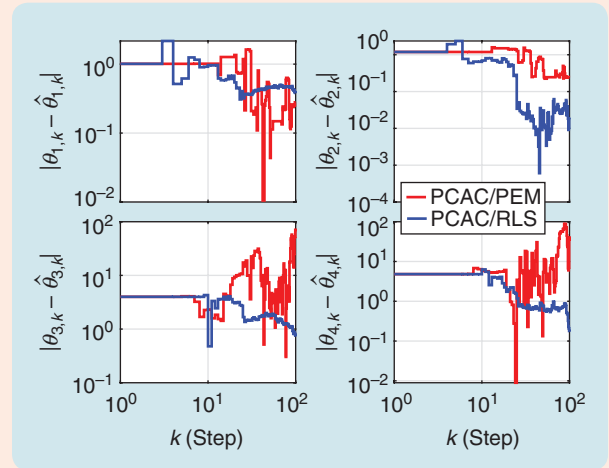


**FIGURE S8** Example S6: Closed-loop identification accuracy of the prediction error method (PEM) and recursive least squares (RLS) operating within predictive cost adaptive control (PCAC)/PEM and PCAC/RLS. Note that neither algorithm is uniformly more accurate.

#### Example S6: An Unstable Plant

Let  $G(z)$  be given by

$$G(z) = \frac{4(z-1.2)}{z^2 - z + 1.2}, \quad (S2)$$

which is unstable, and let  $w_k$  and  $v_k$  be as in Example S3. Figure S7 shows  $y_k$  and  $u_k$  for PCAC/PEM and PCAC/RLS. Figure S8 shows the error of each coefficient of (S2) versus the time step obtained with PEM and RLS operating within PCAC/PEM and RLS in PCAC. Note that PCAC/PEM fails to stabilize the plant.  $\diamond$

the  $i$ -step predicted output is given by

$$y_{i|k} = Cx_{i|k} + \hat{D}_k u_{i|k}, \quad i \geq 2. \quad (31)$$

Note that the  $i$ -step prediction at step  $k$  uses the current estimates  $\hat{A}_k$ ,  $\hat{B}_k$ , and  $\hat{D}_k$  at each intermediate stage of the prediction horizon. It follows that

$$Y_{1|k,\ell} = \hat{\Gamma}_{k,\ell} X_{1|k} + \hat{T}_{k,\ell} U_{1|k,\ell}, \quad (32)$$

where

$$Y_{1|k,\ell} \triangleq \begin{bmatrix} y_{1|k} \\ \vdots \\ y_{\ell|k} \end{bmatrix} \in \mathbb{R}^{\ell p}, \quad U_{1|k,\ell} \triangleq \begin{bmatrix} u_{1|k} \\ \vdots \\ u_{\ell|k} \end{bmatrix} \in \mathbb{R}^{\ell m}, \quad (33)$$

and  $\hat{\Gamma}_{k,\ell} \in \mathbb{R}^{\ell p \times \hat{n}p}$  and  $\hat{T}_{k,\ell} \in \mathbb{R}^{\ell p \times \ell m}$  are the observability and block Toeplitz matrices

$$\hat{\Gamma}_{k,\ell} \triangleq \begin{bmatrix} C \\ C\hat{A}_k \\ \vdots \\ C\hat{A}_k^{\ell-1} \end{bmatrix}, \quad \hat{T}_{k,\ell} \triangleq \begin{bmatrix} \hat{D}_k & 0_{p \times m} & \cdots & \cdots & \cdots & \cdots & 0_{p \times m} \\ \hat{H}_{k,1} & \hat{D}_k & \cdots & \cdots & \cdots & \cdots & 0_{p \times m} \\ \hat{H}_{k,2} & \hat{H}_{k,1} & \hat{D}_k & \cdots & \cdots & \cdots & 0_{p \times m} \\ \hat{H}_{k,3} & \hat{H}_{k,2} & \hat{H}_{k,1} & \hat{D}_k & \cdots & \cdots & 0_{p \times m} \\ \hat{H}_{k,4} & \hat{H}_{k,3} & \hat{H}_{k,2} & \hat{H}_{k,1} & \hat{D}_k & \cdots & \vdots \\ \vdots & \vdots & \vdots & \vdots & \vdots & \ddots & \vdots \\ \hat{H}_{k,\ell-1} & \hat{H}_{k,\ell-2} & \hat{H}_{k,\ell-3} & \cdots & \hat{H}_{k,2} & \hat{H}_{k,1} & \hat{D}_k \end{bmatrix}, \quad (34)$$

where, for all  $i = 1, \dots, \ell - 1$ ,  $\hat{H}_{k,i} \in \mathbb{R}^{p \times m}$  is defined by

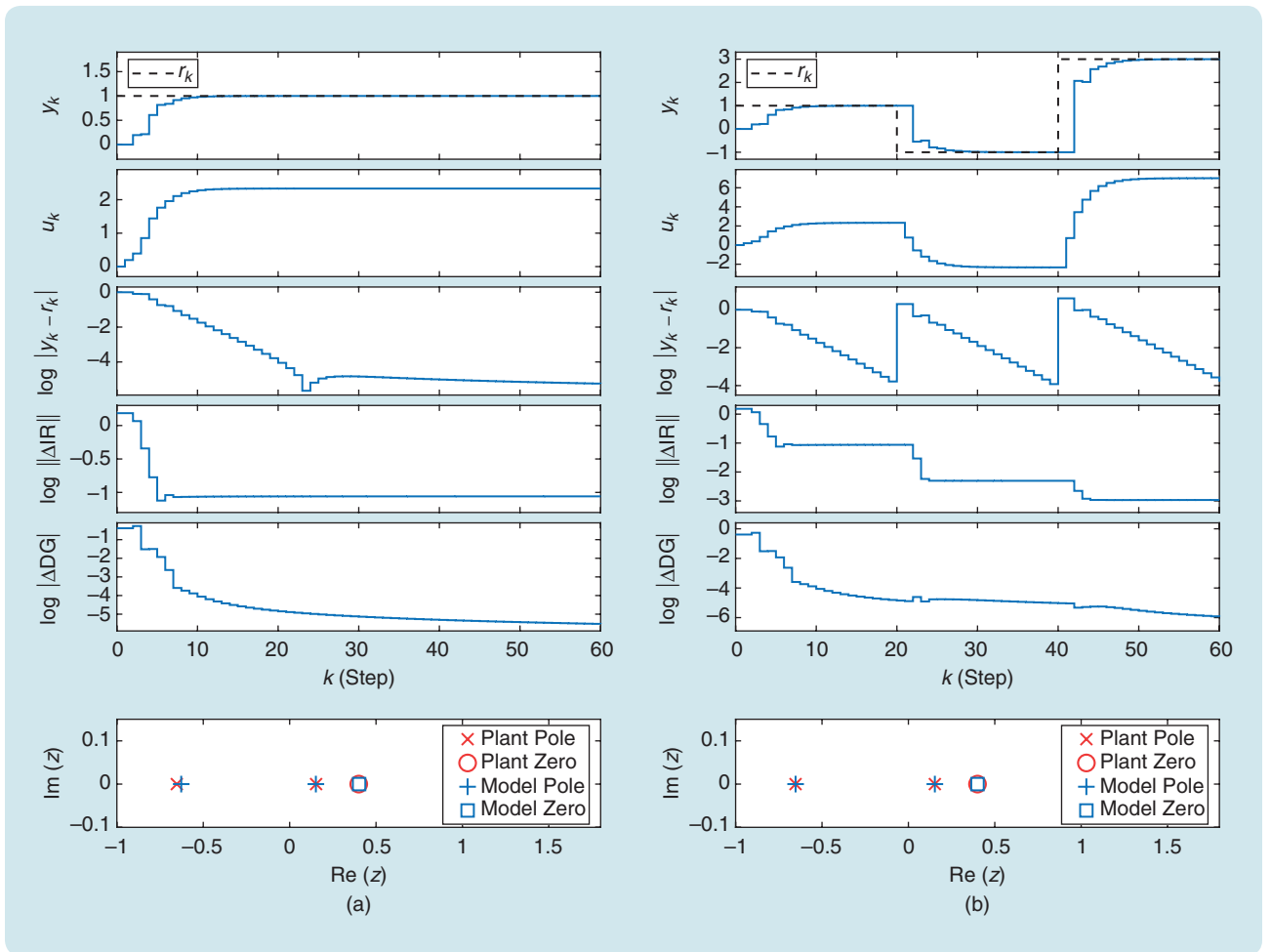


**FIGURE 2** Example 1: Command following for the discrete-time asymptotically stable single-input, single-output plant (46) using  $\hat{n} = n = 2$  with a strictly proper model, that is, with  $\hat{G}_{0,k} = 0$ . (a) The single-step command is  $r_k \equiv 1$ . The output  $y_k$  approaches the step command with a decreasing command-following error, which is  $5.6e-6$  at  $k = 60$ . Note that, although the impulse-response error  $\Delta IR$  stops decreasing after the initial transient, the dc gain estimation error approaches zero, which indicates exogeneity within the closed-loop identification; the identification of the dc gain is prioritized by recursive least squares to decrease the command-following error. The bottom-most plot compares the poles and zero of the identified model at  $k = 60$  to the poles and zero of the plant. (b) The multistep command  $r_k$  is given by (47). For each step command,  $y_k$  approaches the command with a decreasing command-following error, which is  $1.6e-4$  at  $k = 19$ ,  $1.2e-4$  at  $k = 39$ , and  $1.6e-4$  at  $k = 60$ . Note that, although  $\Delta IR$  stops decreasing after each transient, the dc gain estimation error approaches zero. The bottom-most plot compares the poles and zero of the identified model at  $k = 60$  to the poles and zero of the plant.  $\Delta DG$ : the absolute value of the difference between the dc gain of the plant and model;  $\Delta IR$ : the  $L_2$ -norm difference between the 30-step impulse response of the plant and model.

$$\hat{H}_{k,i} \triangleq C\hat{A}_k^{i-1}\hat{B}_k. \quad (35)$$

Let  $\mathcal{R}_{k,\ell} \triangleq [r_{k+1}^T \dots r_{k+\ell}^T]^T \in \mathbb{R}^{\ell p_t}$  be the vector of  $\ell$  future commands; define  $C_{t,\ell} \triangleq I_\ell \otimes C_t \in \mathbb{R}^{\ell p_t \times p_t}$ , let  $Y_{t,1|k,\ell} \triangleq C_{t,\ell} Y_{1|k,\ell}$ , where  $Y_{1|k,\ell}$  is given by (32), be the  $\ell$ -step propagated tracking-output vector; and define the sequence of differences of the computed control inputs by

$$\Delta U_{1|k,\ell} \triangleq [(u_{1|k} - u_k)^T (u_{2|k} - u_{1|k})^T \dots (u_{\ell|k} - u_{\ell-1|k})^T]^T \in \mathbb{R}^{\ell m}. \quad (36)$$

To facilitate the implementation of linear inequality constraints over the horizon  $\ell$ , define  $C_\ell \triangleq I_\ell \otimes (CC_c) \in \mathbb{R}^{\ell n_c \times \ell p}$  and  $\mathcal{D}_\ell \triangleq \mathbf{1}_{\ell \times 1} \otimes \mathcal{D} \in \mathbb{R}^{\ell n_c}$ . With this notation, QP-based receding-horizon optimization is given by:

### Quadratic Programming-Based Receding-Horizon Optimization

$$\min_{U_{1|k,\ell}} (Y_{t,1|k,\ell} - R_{k,\ell})^T Q (Y_{t,1|k,\ell} - R_{k,\ell}) + (\Delta U_{1|k,\ell})^T R \Delta U_{1|k,\ell} \quad (37)$$

subject to

$$C_\ell Y_{1|k,\ell} + \mathcal{D}_\ell \leq 0_{\ell n_c} \quad (38)$$

$$U_{\min} \leq U_{1|k,\ell} \leq U_{\max}, \quad (39)$$

$$\Delta U_{\min} \leq \Delta U_{1|k,\ell} \leq \Delta U_{\max}, \quad (40)$$

where  $Q \triangleq \begin{bmatrix} Q & 0_{p_t \times p_t} \\ 0_{m \times p_t} & P \end{bmatrix} \in \mathbb{R}^{\ell p_t \times \ell p_t}$  is the positive definite output weight;  $\tilde{Q} \in \mathbb{R}^{\ell \times \ell}$  is the positive definite cost-to-go output weight;  $\tilde{P} \in \mathbb{R}^{p_t \times p_t}$  is the positive definite terminal output weight;  $R \in \mathbb{R}^{\ell m \times \ell m}$  is the positive definite control

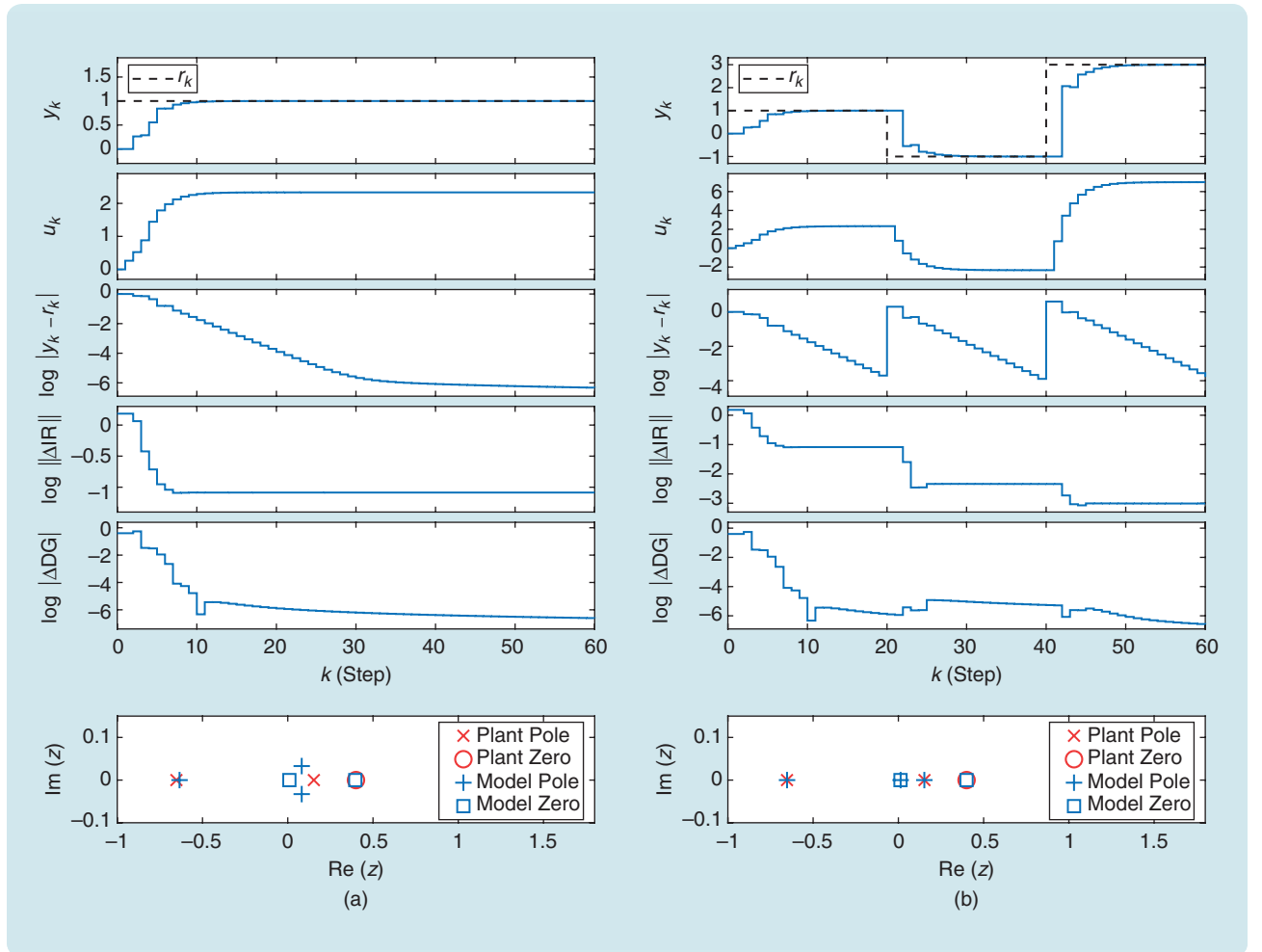


**FIGURE 3** Example 1: Command following for the discrete-time asymptotically stable single-input, single-output plant (46) using  $\hat{n} = 3 > n = 2$  with a strictly proper model. (a) The single-step command is  $r_k \equiv 1$ . The output  $y_k$  approaches the step command with a decreasing command-following error, which is  $4.7e-7$  at  $k = 60$ . (b) The multistep command  $r_k$  is given by (47). For each step command,  $y_k$  approaches the command with a decreasing command-following error, which is  $2e-4$  at  $k = 19$ ,  $1.3e-4$  at  $k = 39$ , and  $1.7e-4$  at  $k = 60$ . Note that, in (b), the estimates of the poles and zeros, including the pole-zero cancellation, are more accurate than in (a) due to the persistency arising from the changing step command.  $\Delta DG$ : the absolute value of the difference between the dc gain of the plant and model;  $\Delta IR$ : the  $L_2$ -norm difference between the 30-step impulse response of the plant and model.

move-size weight;  $U_{\min} \triangleq 1_{\ell \times 1} \otimes u_{\min} \in \mathbb{R}^{\ell m}$ ,  $U_{\max} \triangleq 1_{\ell \times 1} \otimes u_{\max} \in \mathbb{R}^{\ell m}$ ,  $\Delta U_{\min} \triangleq 1_{\ell \times 1} \otimes \Delta u_{\min} \in \mathbb{R}^{\ell m}$ , and  $\Delta U_{\max} \triangleq 1_{\ell \times 1} \otimes \Delta u_{\max} \in \mathbb{R}^{\ell m}$ . Since  $R$  is positive definite, QP-based receding-horizon optimization is a strictly convex optimization problem.

It may occur in practice that the constraint (38) on the predicted output cannot be satisfied for all values of the control input that satisfy (6) and (7). In this case, QP-based receding-horizon optimization is *infeasible*. To overcome this problem, a standard technique is to introduce a slack variable  $\varepsilon \in \mathbb{R}^{\ell n_c}$  to relax the constraint (38). With this modification, the QP-based receding-horizon optimization becomes:

### Quadratic Programming-Based Receding-Horizon Optimization With Output-Constraint Relaxation

$$\min_{U_{1|k,\ell}, \varepsilon} (Y_{t,1|k,\ell} - R_{k,\ell})^T Q (Y_{t,1|k,\ell} - R_{k,\ell}) + (\Delta U_{1|k,\ell})^T R \Delta U_{1|k,\ell} + \varepsilon^T S \varepsilon \quad (41)$$

subject to

$$C_\ell Y_{1|k,\ell} + D_\ell \leq \varepsilon, \quad (42)$$

$$U_{\min} \leq U_{1|k,\ell} \leq U_{\max}, \quad (43)$$

$$\Delta U_{\min} \leq \Delta U_{1|k,\ell} \leq \Delta U_{\max}, \quad (44)$$

$$0_{\ell n_c \times 1} \leq \varepsilon, \quad (45)$$

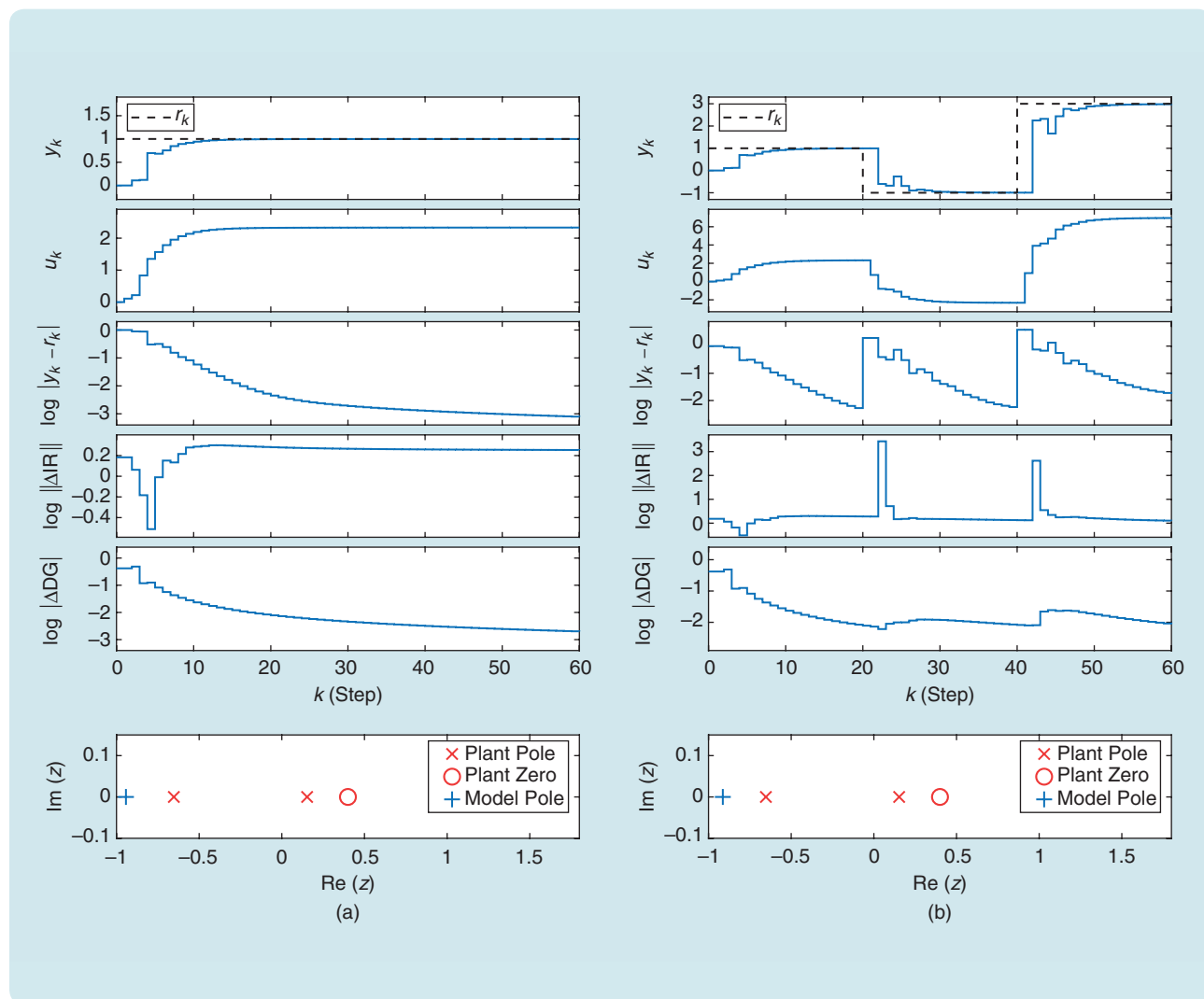


**FIGURE 4** Example 1: Command following for the discrete-time asymptotically stable single-input, single-output plant (46) using  $\hat{n} = 1 < n = 2$  with a strictly proper model. (a) The single-step command is  $r_k \equiv 1$ . The output  $y_k$  approaches the step command with a decreasing command-following error, which is  $7.8\text{e-}4$  at  $k = 60$ . (b) The multistep command  $r_k$  is given by (47). For each step command,  $y_k$  approaches the command with a decreasing command-following error, which is  $5.3\text{e-}3$  at  $k = 19$ ,  $5.7\text{e-}3$  at  $k = 39$ , and  $1.8\text{e-}2$  at  $k = 60$ . Note that the accuracies of the impulse response and the poles and zeros of the identified model in both (a) and (b) are poor, due to the fact that  $\hat{n} < n$ . Nevertheless, in both (a) and (b), the estimate of the dc gain is sufficiently accurate to allow predictive cost adaptive control to approach the step command.  $\Delta DG$ : the absolute value of the difference between the dc gain of the plant and model;  $\Delta IR$ : the  $L_2$ -norm difference between the 30-step impulse response of the plant and model.

where  $S \in \mathbb{R}^{\hat{n}_c \times \hat{n}_c}$  is the positive definite constraint relaxation weight. Since  $R$  and  $S$  are positive definite, (41)–(45) is a strictly convex optimization problem.

The accelerated dual gradient-projection algorithm is used to solve (37)–(40) and (41)–(45), where the previously computed Lagrange multipliers provide a warm start for the next iteration. For real-time implementation, the control computed between  $k$  and  $k + 1$  is implemented at step  $k + 1$ .

### LINEAR SINGLE-INPUT, SINGLE-OUTPUT EXAMPLES

This section considers linear time-invariant SISO plants, where  $y_{t,k} = y_{c,k} = y_k$ . None of the examples in this article consider command preview. In particular, for all command-following

examples,  $R_{k,\ell} = 1_{\ell \times 1} \otimes r_k$ , which implies that future commands over the prediction horizon are assumed to be equal to the current command.

Discrete-time and sampled-data plants are considered in this section. For all sampled-data examples, in this and later sections, the analog-to-digital conversion is an instantaneous sampler, and the digital-to-analog conversion is a zero-order hold (ZOH) device. PCAC is run between sampling times, and the continuous-time dynamics are integrated by ode45 to capture intersample behavior. All commands are discrete-time signals, all deterministic disturbances are discretized at the integration step size, and all stochastic disturbances are modeled as constant between sampling times.

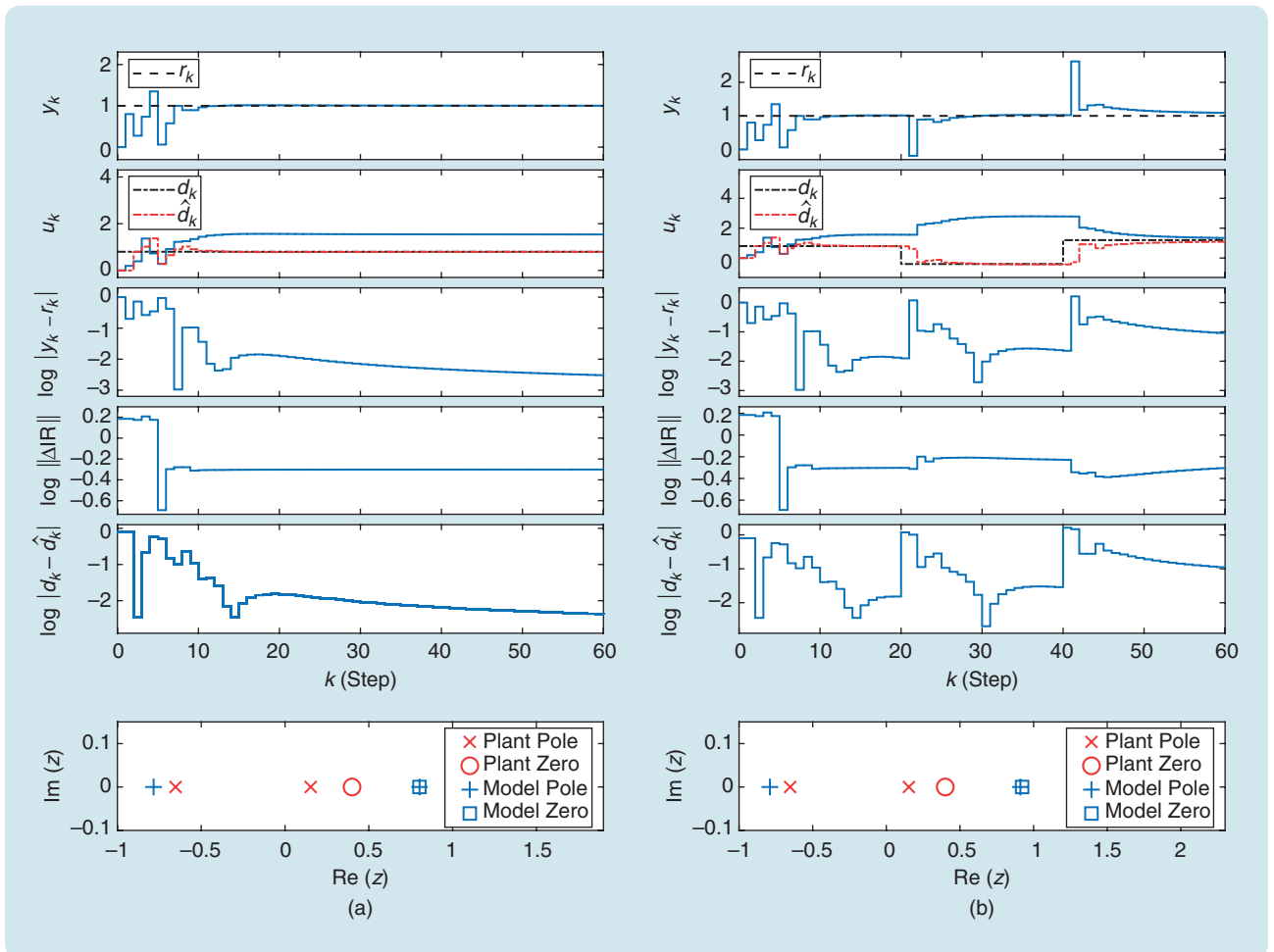


**FIGURE 5** Example 1: Command following and disturbance rejection for the discrete-time asymptotically stable single-input, single-output plant (46) using  $r_k \equiv 1$  and  $\hat{n} = n = 2$  with a strictly proper model. (a) The single-step disturbance is  $d_k \equiv 0.8$ . The output  $y_k$  approaches the step command with a decreasing command-following error, which is  $3e-3$  at  $k = 60$ . Note that, although  $\Delta IR$  stops decreasing after the initial transient, recursive least squares (RLS) continues to refine the estimate  $\hat{d}_k$  of the disturbance for the remainder of the simulation. This refinement indicates exigency within the closed-loop identification, where the estimation of  $\hat{d}_k$  is prioritized to decrease the command-following error. The bottom-most plot shows a pole-zero cancellation in the identified model at  $k = 60$ . (b) The multistep disturbance  $d_k$  is given by (52). For each step disturbance,  $y_k$  approaches the command with a decreasing command-following error, which is  $1.3e-2$  at  $k = 19$ ,  $2.4e-2$  at  $k = 39$ , and  $8.8e-2$  at  $k = 60$ . Note that, although  $\Delta IR$  stops decreasing within a few steps after each change in the disturbance, RLS continues to refine the estimate  $\hat{d}_k$  of the disturbance while  $d_k$  is constant. Note that, in both (a) and (b), the step disturbances induce self-generated persistency, which facilitates the ability of RLS to effectively construct an estimate  $\hat{d}_k$  of the disturbance  $d_k$ , which, in turn, facilitates disturbance rejection. The bottom-most plot shows a pole-zero cancellation in the identified model at  $k = 60$ , due to the step disturbance.  $\Delta IR$ : the  $L_2$ -norm difference between the 30-step impulse response of the plant and model.

All of the subsequent examples involving PCAC are based on RLS for closed-loop identification. "Open- and Closed-Loop Identification Using the Prediction Error Method and Instrumental Variables" compares the accuracy of PEM and IV with RLS for open-loop identification as well as for closed-loop identification with a linear time-invariant controller. In addition, "Closed-Loop Identification Under Predictive Cost Adaptive Control With the Prediction Error Method" compares the performance of PCAC using PEM and RLS for PCAC control, where the identified plant model is updated at each step.

### Example 1: A Discrete-Time Asymptotically Stable Minimum-Phase Plant

The goal of this example is to investigate the ability of PCAC to follow step commands and reject step disturbances for an asymptotically stable minimum-phase plant for various choices

of model order  $\hat{n}$ . Consider the discrete-time input-output SISO plant

$$y_k = -0.5y_{k-1} + 0.1y_{k-2} + u_{k-1} - 0.4u_{k-2}. \quad (46)$$

Let  $u_{\min} = -10$ ,  $u_{\max} = 10$ ,  $\Delta u_{\min} = -10$ ,  $\Delta u_{\max} = 10$ , and  $v_k = 0$ . No output constraint is considered in this example. The plant (46) is initialized with  $y_{-1} = y_{-2} = 0$  and  $u_0 = u_{-1} = u_{-2} = 0$ . Note that the order of the plant is  $n = 2$ . At each time step, PCAC uses (37)–(40) with  $\ell = 5$ ,  $\hat{Q} = 2I_{\ell-1}$ ,  $\hat{P} = 5$ , and  $R = I_{\ell}$ . Let  $\lambda = 1$ ,  $\theta_0 = 10^{-2} \cdot 1_{2\hat{n} \times 1}$ , and  $P_0 = 10^3 I_{2\hat{n}}$ .

Figures 2–4 show the response of PCAC for  $\hat{n} = 2$ ,  $\hat{n} = 3$ , and  $\hat{n} = 1$ , respectively, using a strictly proper model, that is, using  $\hat{G}_{0,k} = 0$ . The absolute value of the command-following error, the  $L_2$ -norm difference between the 30-step impulse response of the plant and model ( $\Delta IR$ ), the absolute value of the

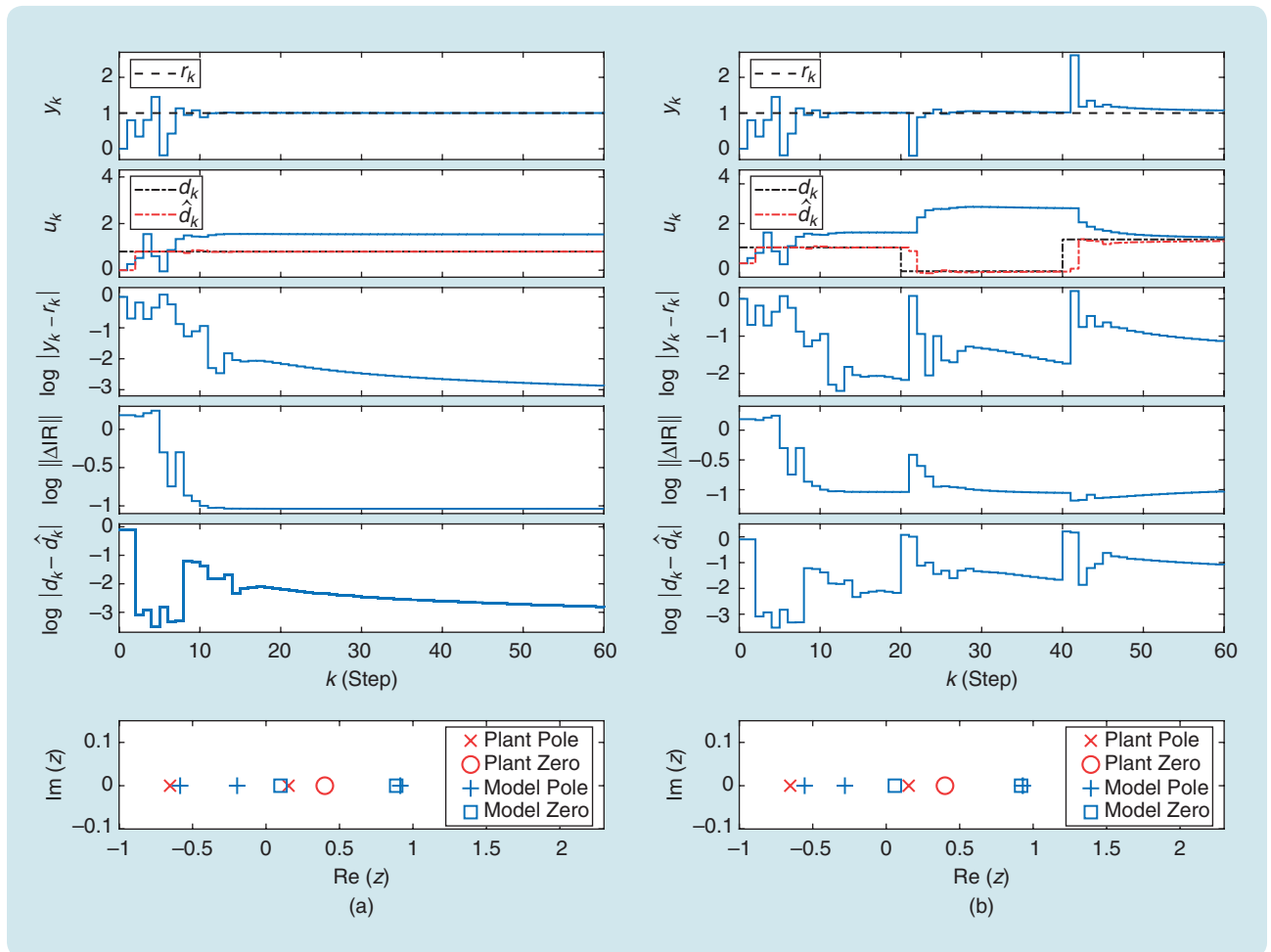


**FIGURE 6** Example 1: Command following and disturbance rejection for the discrete-time asymptotically stable single-input, single-output plant (46) using  $r_k \equiv 1$  and  $\hat{n} = 3 > n = 2$  with a strictly proper model. (a) The single-step disturbance is  $d_k \equiv 0.8$ . The output  $y_k$  approaches the step command with a decreasing command-following error, which is  $1.3e-3$  at  $k = 60$ . (b) The multistep disturbance  $d_k$  is given by (52). For each step disturbance,  $y_k$  approaches the command with a decreasing command-following error, which is  $7.4e-3$  at  $k = 19$ ,  $2e-2$  at  $k = 39$ , and  $7.1e-2$  at  $k = 60$ . Note that, although the accuracies of the poles and zeros of the identified model in both (a) and (b) are poor, the estimate of the disturbance is sufficiently accurate to allow predictive cost adaptive control to approach the command and reject the disturbance.  $\Delta IR$ : the  $L_2$ -norm difference between the 30-step impulse response of the plant and model.

difference between the dc gain of the plant and model ( $\Delta DG$ ), and the pole-zero location of the plant and model identified at  $k = 60$  are computed as diagnostics. Figures 2(a), 3(a), and 4(a) show the response of PCAC for the constant command  $r_k \equiv 1$ , and Figures 2(b), 3(b), and 4(b) show the response of PCAC for the three-step command

$$r_k = \begin{cases} 1, & 0 \leq k < 20, \\ -1, & 20 \leq k < 40, \\ 3, & k \geq 40. \end{cases} \quad (47)$$

Figures 2–4 show that, for asymptotically stable minimum-phase plants, PCAC follows step commands and is robust to the choice of model order  $\hat{n}$ .

Next, a matched disturbance  $d_k \in \mathbb{R}$  is applied to the plant (46), for which the plant output is given by

$$y_k = -\sum_{i=1}^n F_i y_{k-i} + \sum_{i=1}^n G_i (u_{k-i} + d_{k-i}), \quad (48)$$

where  $n = 2$ ,  $F_1 = 0.5$ ,  $F_2 = -0.1$ ,  $G_1 = 1$ , and  $G_2 = -0.4$ . In the case of a constant matched disturbance  $\hat{d}_k \in \mathbb{R}$ , the plant output is given by

$$y_k = -\sum_{i=1}^n F_i y_{k-i} + \sum_{i=1}^n G_i u_{k-i} + \sum_{i=1}^n G_i \hat{d}_k, \quad (49)$$

and for a given model order  $\hat{n}$ , the output of the model identified by RLS at step  $k$  is given by

$$y_k = -\sum_{i=1}^{\hat{n}} \hat{F}_{i,k} y_{k-i} + \sum_{i=1}^{\hat{n}} \hat{G}_{i,k} u_{k-i}. \quad (50)$$

Using (50) in (49), the disturbance  $\hat{d}_k$  estimated by RLS is given by

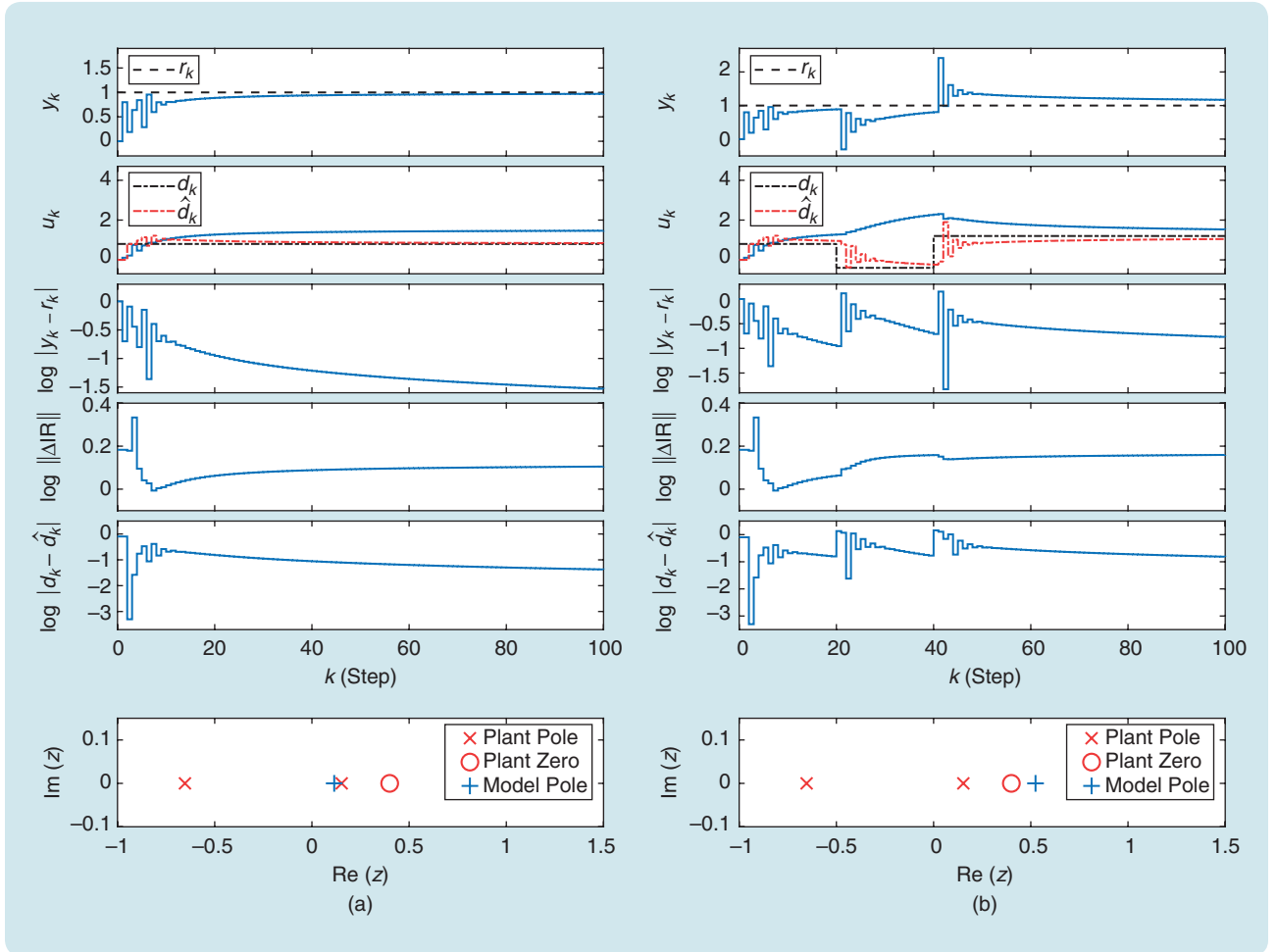


**FIGURE 7** Example 1: Command following and disturbance rejection for the discrete-time asymptotically stable single-input, single-output plant (46) using  $r_k \equiv 1$  and  $\hat{n} = 1 < n = 2$  with a strictly proper model. (a) The single-step disturbance is  $d_k \equiv 0.8$ . The output  $y_k$  approaches the step command with a decreasing command-following error, which is  $2.9e-2$  at  $k = 100$ . (b) The multistep disturbance  $d_k$  is given by (52). For each step disturbance,  $y_k$  approaches the command with a decreasing command-following error, which is  $1.2e-1$  at  $k = 19$ ,  $2.1e-1$  at  $k = 39$ , and  $1.7e-1$  at  $k = 100$ . Note that, in both (a) and (b),  $y_k$  approaches the command more slowly than in the cases  $\hat{n} = 2$  and  $\hat{n} = 3$  considered in Figures 5 and 6, respectively.  $\Delta IR$ : the  $L_2$ -norm difference between the 30-step impulse response of the plant and model.

$$\hat{d}_k = \left[ -\sum_{i=1}^{\hat{n}} \hat{F}_{i,k} y_{k-i} + \sum_{i=1}^{\hat{n}} \hat{G}_{i,k} u_{k-i} + \sum_{i=1}^n F_i y_{k-i} - \sum_{i=1}^n G_i u_{k-i} \right] \sum_{i=1}^n G_i^{-1}. \quad (51)$$

Figures 5–7 show the response of PCAC for  $\hat{n}=2$ ,  $\hat{n}=3$ , and  $\hat{n}=1$ , respectively, with constant command  $r_k \equiv 1$ , where the error of the disturbance estimate  $\hat{d}_k$  is computed. In Figures 5(a), 6(a), and 7(a), the constant disturbance  $d_k \equiv 0.8$  is applied, and in Figures 5(b), 6(b), and 7(b), the three-step disturbance

$$d_k = \begin{cases} 0.8, & 0 \leq k < 20, \\ -0.4, & 20 \leq k < 40, \\ 1.2, & k \geq 40 \end{cases} \quad (52)$$

is applied. Figures 5–7 show that, for the asymptotically stable minimum-phase plant (46), PCAC rejects step disturbances with  $\hat{n} \geq n$ . Note that self-generated persistency is evident in the control input arising from the step-command changes and step disturbances. Furthermore, it is seen that, although the impulse-response error  $\Delta IR$  stops decreasing after each transient, RLS keeps refining the dc gain of the model for the remainder of the simulation. This indicates exigency within identification, as RLS prioritizes the identification of the dc gain over the impulse response to achieve command following.  $\diamond$

Example 1 showed that PCAC can follow step commands and reject step disturbances. This ability is further investigated within the context of fixed-gain integral control in “Following Step Commands Without an Integrator.”

## Following Step Commands Without an Integrator

Since receding-horizon optimization determines control inputs without using an explicit feedback controller, it is desirable to compare the performance of predictive cost adaptive control (PCAC) with the performance of linear time-invariant controllers. In particular, within the context of linear time-invariant control, asymptotic step-command following is achievable if and only if the controller or plant includes an integrator. To investigate asymptotic step-command following under PCAC, the performance of PCAC using online identification is com-

pared with linear time-invariant integral control as well as with PCAC using a fixed model with erroneous dc gain. To do this, consider the discrete-time plants

$$G(z) = \frac{z-0.5}{(z-0.2)(z-0.8)}, \quad (S3)$$

$$G(z) = \frac{0.1(z-0.5)}{(z-0.2)(z-0.8)}, \quad (S4)$$

$$G(z) = \frac{5(z-0.5)}{(z-0.2)(z-0.8)}, \quad (S5)$$

$$G(z) = \frac{0.1953(z-0.2)}{(z-0.5)(z-0.9)}, \quad (S6)$$

which are asymptotically stable and have dc gains 3.125, 0.3125, 15.625, and 3.125, respectively. Note that (S3)–(S5) have the same poles and zeros and that (S3) and (S6) have the same dc gains but different poles and zeros. Disturbance and sensor noise are not considered in these examples. A strictly proper model is used for identification in PCAC; that is,  $\hat{G}_{0,k} = 0$  is enforced.

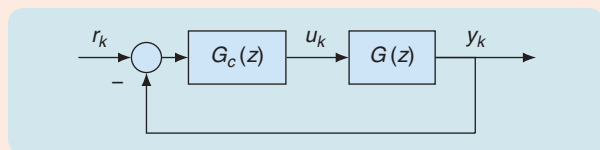


FIGURE S9 Basic servo loop with step command  $r_k$  and integral controller  $G_c$ .

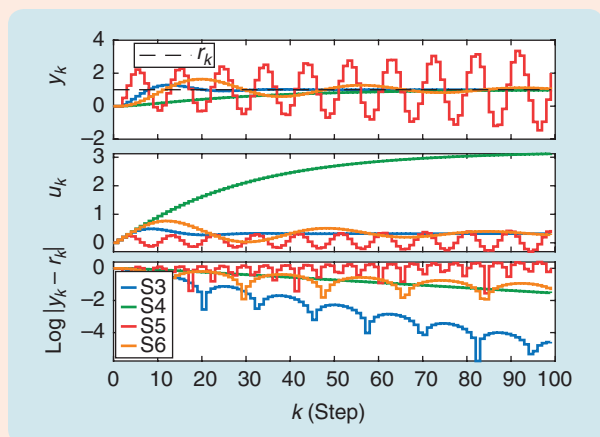


FIGURE S10 Example S7: Linear time-invariant integral control for  $G(z)$  given by (S4)–(S6) with the controller (S7). For plants (S3), (S4), and (S6), the closed-loop system is asymptotically stable, and, thus, asymptotic step-command following is achieved. For the plant (S5), the closed-loop system is unstable.

### Example S7: Linear Time-Invariant Integral Control

Consider the basic servo loop shown in Figure S9 with the integral controller

$$G_c(z) = \frac{0.1}{z-1}. \quad (S7)$$

Figure S10 shows the closed-loop response with the controller (S7) and plants (S3)–(S6). The closed-loop dynamics are asymptotically stable for  $G(z)$  given by (S3), (S4), and (S6), and, thus, the command-following error converges to zero. On the other hand, the closed-loop dynamics are unstable for  $G(z)$  given by (S5), and, thus,  $y_k$  diverges.  $\diamond$

### Example S8: Predictive Cost Adaptive Control With Fixed Models

Let the true plant  $G(z)$  be given by (S3). PCAC is applied with the fixed models (S3)–(S6) with  $u_{\min} = -1$ ,  $u_{\max} = 1$ ,  $\Delta u_{\min} = -1$ ,  $\Delta u_{\max} = 1$ ,  $\ell = 50$ ,  $\bar{Q} = I_{\ell-1}$ ,  $\bar{P} = 1$ , and  $R = I_{\ell}$ . Figure S11 shows that the command-following error approaches zero in the cases where

### Example 2: A Discrete-Time Unstable Nonminimum-Phase Plant

The goal of this example is to investigate the ability of PCAC to follow step commands for various choices of initial models; various levels of zero-mean, Gaussian white sensor noise; and various model orders  $\hat{n}$ . Furthermore, this example compares the identification accuracy of RLS within PCAC and in the case where the closed-loop data are from an LQG controller with a built-in integrator. Consider the discrete-time input-output SISO plant

$$y_k = 1.4y_{k-1} - 0.3y_{k-2} + u_{k-1} - 1.3u_{k-2}. \quad (53)$$

Let  $u_{\min} = -50$ ,  $u_{\max} = 50$ ,  $\Delta u_{\min} = -10$ ,  $\Delta u_{\max} = 10$ , and  $v_k = 0$ . No output constraint is considered in this example. The

plant (53) is initialized with  $y_{-1} = y_{-2} = 0$  and  $u_0 = u_{-1} = u_{-2} = 0$ . At each time step, PCAC uses (37)–(40) with  $\ell = 20$ ,  $\bar{Q} = 2I_{\ell-1}$ ,  $\bar{P} = 5$ , and  $R = I_\ell$ . Let  $\lambda = 1$  and  $P_0 = 10^3 I_{2\hat{n}}$ .

Figure 8 shows the response of PCAC for  $\hat{n} = n = 2$  using a strictly proper model, where  $\theta_0 = \alpha[0 \ 0 \ 0 \ 1]^T$ ,  $\alpha \in \{-10, -1, -0.1, 0.1, 1, 10\}$ . Note that the initial model is a finite-impulse response (FIR) model. Figure 8(a) uses the constant command  $r_k \equiv 1$ , and Figure 8(b) uses the three-step command  $r_k$  given by (47).

Figure 9 shows the response of PCAC for  $r_k \equiv 1$  and  $\hat{n} = n = 2$  using a strictly proper model with a randomly chosen initial estimate  $\theta_0$ . In particular, in Figure 9, parts(a) and (b) each shows 100 responses of PCAC with  $\theta_0$  sampled from a zero-mean, Gaussian distribution with standard deviations of one and two, respectively.

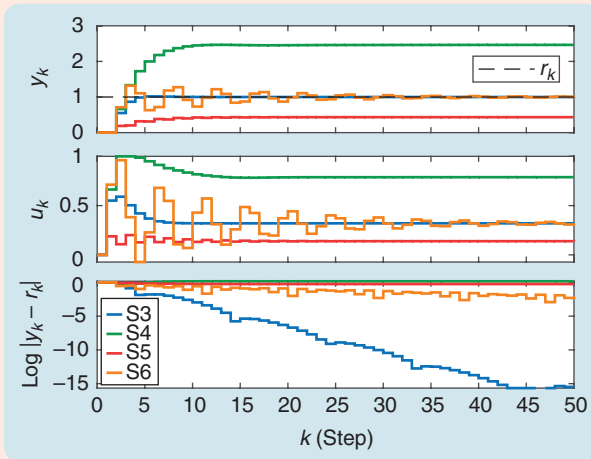


**FIGURE S11** Example S8: Step-command following using predictive cost adaptive control with fixed models (S3)–(S6). Asymptotic command following is achieved in the cases (S3) and (S6), where the dc gain of the model is the same as the dc gain of the plant. Note that asymptotic command following is achieved in the case of (S6) despite the fact that all of the poles and zeros of the fixed model are incorrect relative to the true plant (S3). For (S4) and (S5), where the dc gain of the model is not equal to the dc gain of the plant, the command-following error remains bounded but does not approach zero.

PCAC uses the fixed models (S3) and (S6), both of which have the correct dc gain. However, in the case where PCAC uses the fixed models (S4) and (S5), both of which have an incorrect dc gain, the command-following error remains bounded but does not approach zero.  $\diamond$

### Example S9: Predictive Cost Adaptive Control With Various Initial Models That Are Different From the True Plant

Let the true plant  $G(z)$  be given by (S3). PCAC is applied with  $u_{\min} = -1$ ,  $u_{\max} = 1$ ,  $\Delta u_{\min} = -1$ ,  $\Delta u_{\max} = 1$ ,  $\ell = 50$ ,  $\bar{Q} = I_{\ell-1}$ ,

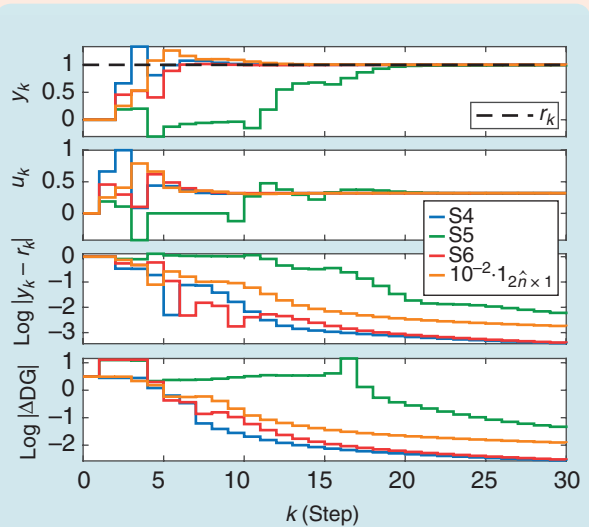


**FIGURE S12** Example S9: Step-command following using predictive cost adaptive control with the initial models (S4)–(S6) as well as the initial model given by  $\theta_0 = 10^{-2} \mathbf{1}_{2\hat{n} \times 1}$ . For all four initial models, the command-following error approaches zero.  $\Delta DG$ : the absolute value of the difference between the dc gain of the plant and model.

$\bar{P} = 1$ ,  $R = I_\ell$ ,  $\lambda = 1$ ,  $\hat{n} = 2$ , and  $P_0 = 10^3 I_{2\hat{n}}$  for the initial models (S4)–(S6) as well as the initial model given by  $\theta_0 = 10^{-2} \mathbf{1}_{2\hat{n} \times 1}$ . Figure S12 shows that, for all four initial models, the command-following error approaches zero. Furthermore, the dc gain of the identified model approaches the dc gain of (S3).  $\diamond$

These examples demonstrate that using  $(\Delta U_{1|k,\ell})^T R \Delta U_{1|k,\ell}$  in (41) does not yield integral action, and, in addition, that estimation of the dc gain of the plant is necessary for asymptotic step-command following.

Next, let  $v_k$  be a zero-mean, Gaussian white noise sequence. In particular, in Figure 10, parts(a) and (b) each shows the response of PCAC using  $r_k \equiv 1$ , the strictly proper FIR model  $\theta_0 = [0^T_{(2\hat{n}-1) \times 1} 1]^T$  with  $\hat{n} = 2$ ,  $\hat{n} = 3$ , and  $\hat{n} = 4$ , for  $v_k$  with standard deviations of 0.05 and 0.15, respectively. Figure 11 shows the accuracy of the model identified by RLS as the standard deviation of  $v_k$  increases for  $\hat{n} \in \{1, 2, \dots, 6\}$  with  $u_k$  given by receding-horizon optimization and LQG with a built-in integrator. The accuracy of the model is determined by  $\Delta\text{IR}$  at  $k = 140$  averaged over 100 simulation runs.

Figures 8–10 show that, for the unstable nonminimum-phase (NMP) plant (53), the output approaches the step commands despite the presence of bias in the estimation of the model coefficients. Figure 11 shows  $\Delta\text{IR}$ , and, thus, the predictive error of the identified model is smaller with RLS within PCAC than with RLS that uses data from an

LQG controller with an integrator. This implies that self-generated persistency facilitates improvement in the identification accuracy.  $\diamond$

### Example 3: An Unstably Stabilizable Plant

The goal of this example is to investigate the ability of PCAC to stabilize unstably stabilizable plants. Consider the discrete-time unstable SISO plant

$$G(z) = \frac{(z - 1.1)(z - 0.4)}{(z - 1.2)(z^2 + 1.2z + 0.57)}. \quad (54)$$

Note that the order of the plant is  $n = 3$ , and its relative degree is one. The damping ratio and natural frequency of the complex poles of (54) are approximately 0.1 and  $0.8\pi$  rad/step, respectively. Since there is an unstable pole on the right side of an

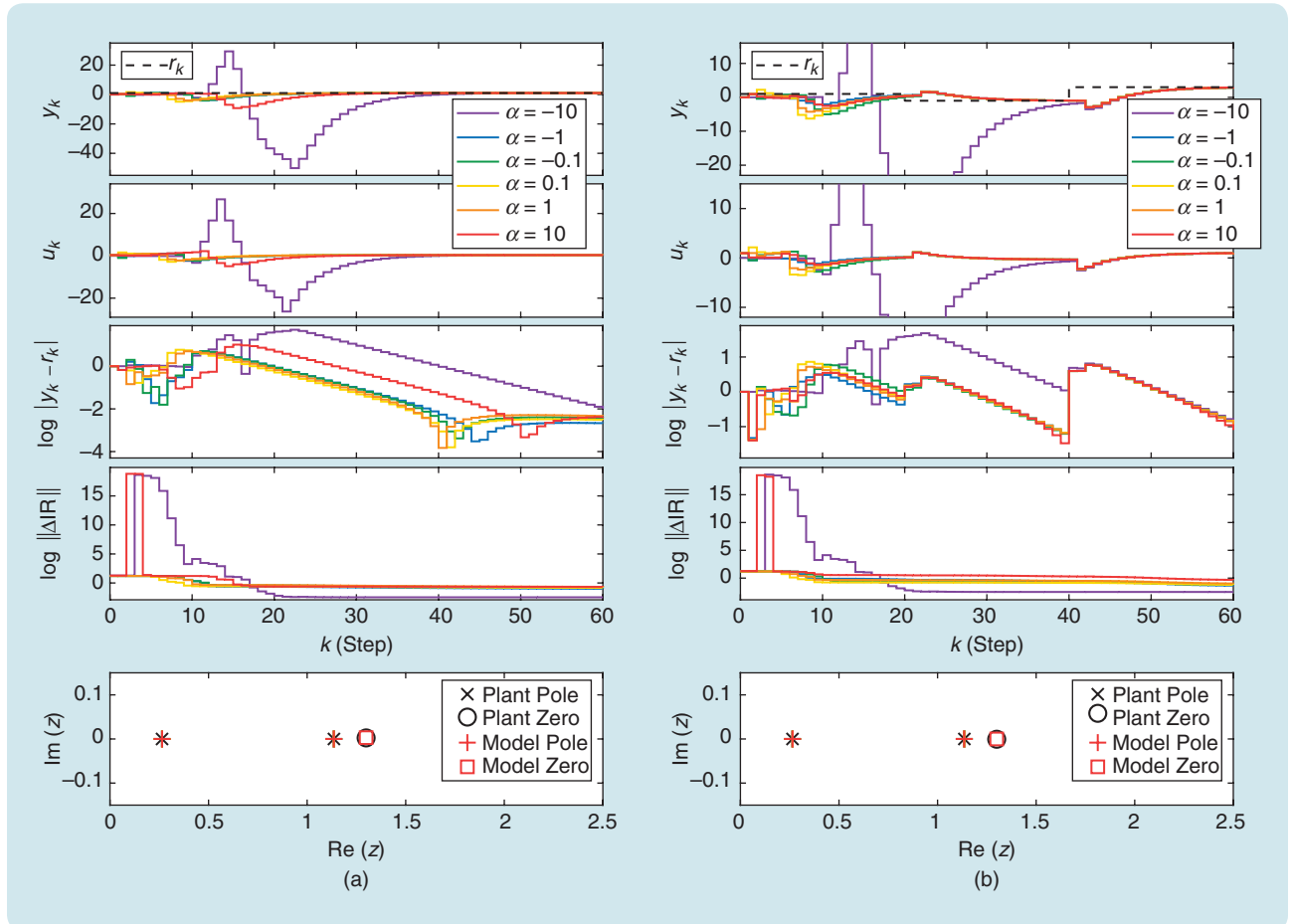


**FIGURE 8** Example 2: Command following for the discrete-time unstable nonminimum-phase single-input, single-output plant (53) using  $r_k \equiv 1$  and  $\hat{n} = n = 2$  with a strictly proper finite-impulse response model initialized with  $\theta_0 = \alpha[0 \ 0 \ 0 \ 1]^T$ ,  $\alpha \in \{-10, -1, -0.1, 0.1, 1, 10\}$ . (a) The single-step command is  $r_k \equiv 1$ . The output  $y_k$  approaches the step command with a decreasing command-following error, which is in the interval  $[2.1e-3, 1.0e-2]$  at  $k = 60$ . Note that, for all  $\alpha$ ,  $\Delta\text{IR}$  approaches asymptotic values for  $k \geq 25$ . The bottom-most plot compares the poles and zero of the identified model at  $k = 60$  to the poles and zero of the plant. (b) The multistep command  $r_k$  is given by (47). For  $\alpha \neq -10$ ,  $y_k$  approaches the three-step command with a decreasing command-following error, which is in the interval  $[4.3e-1, 1.1]$  at  $k = 19$ ,  $[3.3e-2, 6.7e-2]$  at  $k = 39$ , and  $[8e-2, 1.2e-1]$  at  $k = 60$ . For  $\alpha = -10$ ,  $y_k$  approaches the last command with a decreasing command-following error, which is  $1.3e-1$  at  $k = 60$ . Note that, for all  $\alpha$ ,  $\Delta\text{IR}$  approaches asymptotic values for  $k \geq 25$ . The bottom-most plot compares the poles and zero of the identified model at  $k = 60$  to the poles and zero of the plant.  $\Delta\text{IR}$ : the  $L_2$ -norm difference between the 30-step impulse response of the plant and model.

NMP zero, pole-zero interlacing fails in the open right-half plane, and, thus, the plant is unstably stabilizable. That is, it can be stabilized by a discrete-time unstable linear time-invariant controller but cannot be stabilized by a discrete-time asymptotically stable linear time-invariant controller [73].

Let  $u_{\min} = -50$ ,  $u_{\max} = 50$ ,  $\Delta u_{\min} = -10$ ,  $\Delta u_{\max} = 10$ ,  $\ell = 50$ ,  $\bar{Q} = 4I_{\ell-1}$ ,  $\bar{P} = 4$ ,  $R = I_{\ell}$ ,  $\lambda = 1$ ,  $P_0 = 10^3 I_{2\hat{n}}$ , and  $\theta_0 = [0_{(2\hat{n}-1) \times 1}^T \ 1]^T$ . A strictly proper model is used for identification in PCAC. No output constraint is considered in this example. The plant is initialized with  $y_{-1} = -0.4$ ,  $y_{-2} = 0.3$ , and  $u_{-1} = u_{-2} = u_{-3} = 0$ . PCAC uses (37)–(40), where the standard deviation of the sensor noise  $v_k$  is 0.02. In this and the following examples, identification and control do not commence until the regressor matrix  $\phi_k$  given by (15) is populated with  $\hat{n}$  measurements. Figure 12(a) shows the response of PCAC for the discrete-time plant (54) for  $\hat{n} = n = 3$  using the three-step command

$$r_k = \begin{cases} 1, & 0 \leq k < 100, \\ -1, & 100 \leq k < 200, \\ 2, & k \geq 200. \end{cases} \quad (55)$$

Next, consider the continuous-time SISO plant

$$G(s) = \frac{(s - 0.1)(s + 0.6)}{(s - 0.2)(s^2 + 2\zeta\omega_n s + \omega_n^2)}, \quad (56)$$

where  $\zeta = 0.1$  and  $\omega_n = 0.8\pi$ . Note that, as in the case of the discrete-time plant (54), the continuous-time plant (56) can be stabilized by a continuous-time unstable linear time-invariant controller but cannot be stabilized by a continuous-time asymptotically stable linear time-invariant controller [73]. With the sample period  $T_s = 1$  s, Figure 12 shows that the ZOH-discretized plant has the same dynamics as the discrete-time

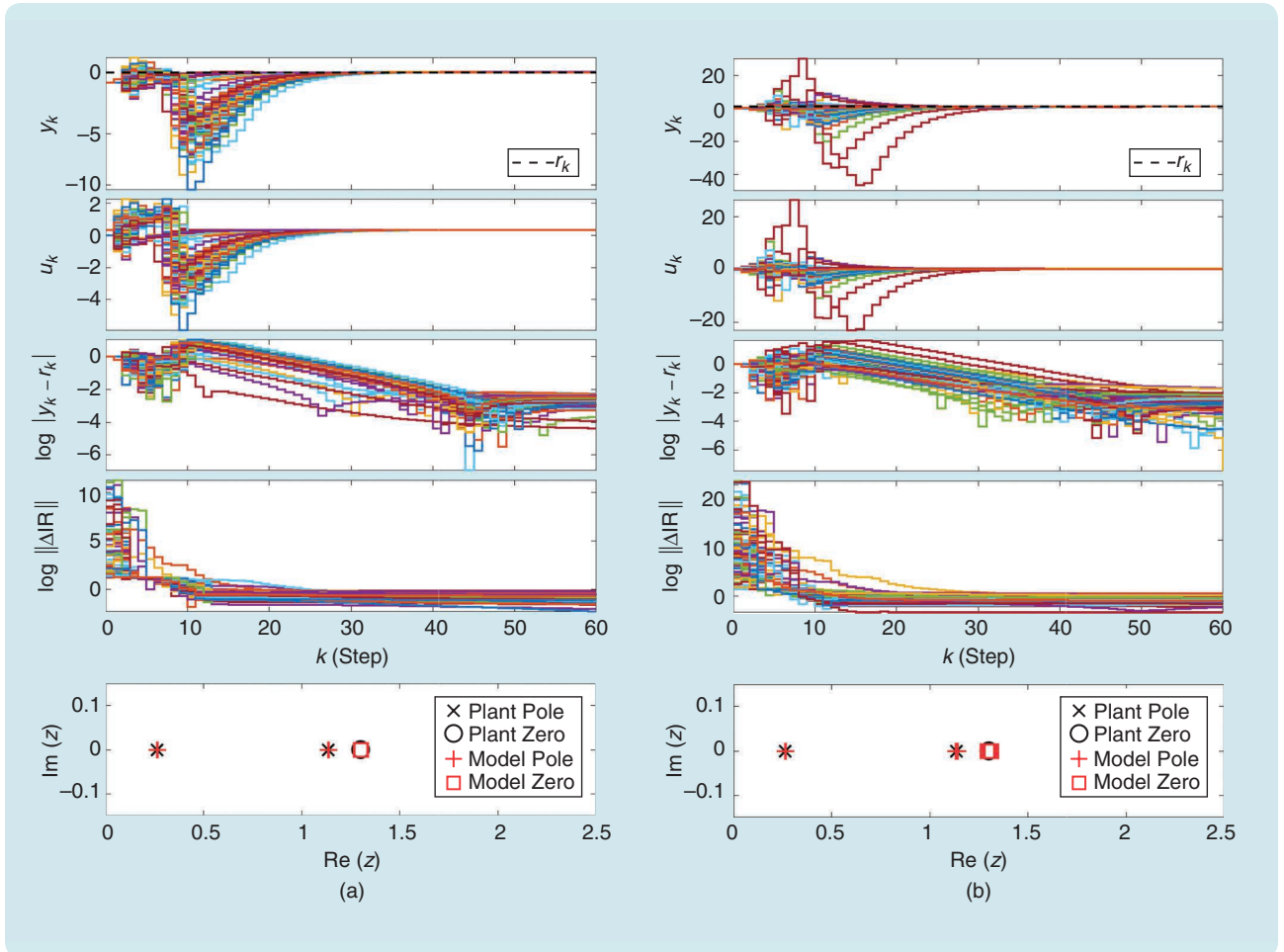


**FIGURE 9** Example 2: Command following for the discrete-time unstable nonminimum-phase single-input, single-output plant (53) using  $r_k \equiv 1$  and  $\hat{n} = n = 2$  with a strictly proper model, which is initialized with 100 Gaussian-distributed samples of  $\theta_0$  with a standard deviation of  $\sigma$ . (a) For  $\sigma = 1$ , the output  $y_k$  approaches the step command with a decreasing command-following error, which is in the interval  $[9.5e-4, 5.5e-3]$  at  $k = 60$ . (b) For  $\sigma = 2$ , the output  $y_k$  approaches the step command with a decreasing command-following error, which is in the interval  $[6.7e-3, 2.1e-2]$  at  $k = 60$ . Note that, in both (a) and (b), although  $\Delta IR$  approaches an asymptotic value for  $k \geq 25$ , indicating the presence of bias and, thus, lack of consistency in the estimate of the model, the poles and zero of the model are close to the poles and zero of the plant at  $k = 60$ .  $\Delta IR$ : the  $L_2$ -norm difference between the 30-step impulse response of the plant and model.

plant (54) and, thus, is not stabilizable by a discrete-time asymptotically stable linear time-invariant controller. The plant is initialized with  $x(0) = [0.4 \ -0.8 \ 1.1]^T$ , where  $x(0)$  is the initial state of the realization

$$\dot{x} = \begin{bmatrix} -0.3027 & -3.1 & 0.6317 \\ 2 & 0 & 0 \\ 0 & 1 & 0 \end{bmatrix} x + \begin{bmatrix} 1 \\ 0 \\ 0 \end{bmatrix} u, \quad (57)$$

$$y = [1 \ 0.25 \ -0.03]x. \quad (58)$$

Figure 12(b) shows the response of PCAC for the continuous-time plant (56) using the same setup as for the discrete-time plant (54). Figure 12 shows that PCAC stabilizes the discrete-time (54) and sampled-data (56) unstably stabilizable plants. Since the plant is unstable, an FIR initial model—all of whose poles are zero—is a poor choice. Consequently, choosing a large optimization horizon yields poor model predictions, which, in turn, yield a large initial transient response. This example suggests that, for unstable plants, it is advisable to avoid choosing large values of the prediction horizon  $\ell$ .  $\diamond$

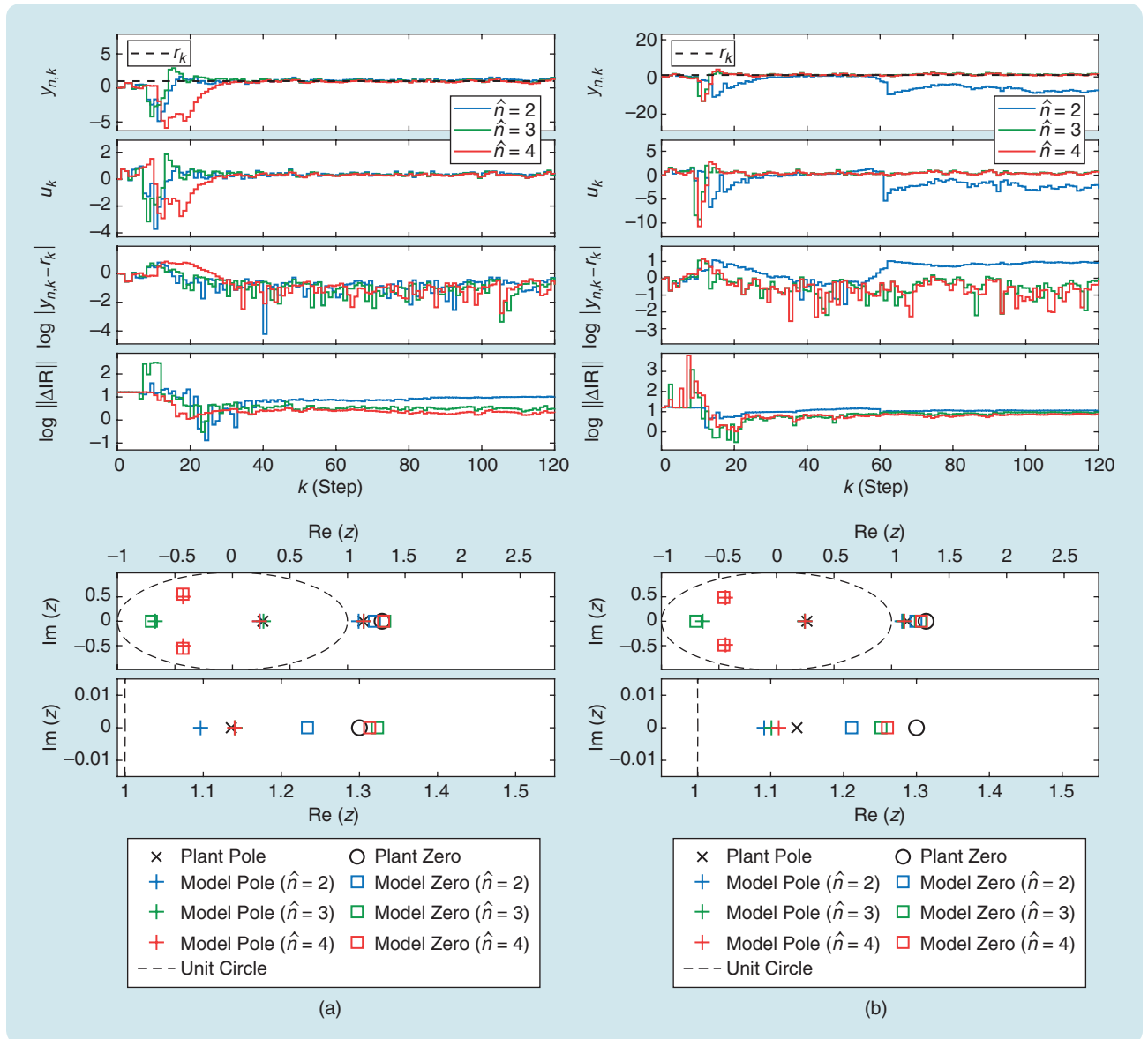


**FIGURE 10** Example 2: Command following for the discrete-time unstable nonminimum-phase single-input, single-output plant (53) using  $r_k \equiv 1$ ; noisy measurement with a noise standard deviation of  $\sigma$ ; and finite-impulse response strictly proper initial model  $\theta_0 = [0_{(2\hat{n}-1) \times 1} \ 1]^T$ , where  $\hat{n} = 2, \hat{n} = 3$ , and  $\hat{n} = 4$ . (a) For  $\sigma = 0.05$ , in all cases,  $y_k$  approaches the step command with a decreasing command-following error. (b) For  $\sigma = 0.15$ ,  $y_k$  approaches the step command with a decreasing command-following error for  $\hat{n} = 3$  and  $\hat{n} = 4$ . For  $\hat{n} = 2$ ,  $y_k$  does not approach the step command, and the command-following error is 7.9 at  $k = 120$ . Note that, in both (a) and (b), larger values of  $\hat{n}$  yield smaller values of  $\Delta IR$ . The bottom-most plots show that larger values of  $\hat{n}$  facilitate identification, and the poles and zero of the model are closer to the poles and zero of the plant.  $\Delta IR$ : the  $L_2$ -norm difference between the 30-step impulse response of the plant and model.

#### Example 4: An Asymptotically Stable Continuous-Time Plant

The goal of this example is to investigate the application of PCAC for sampled-data control with harmonic and broadband disturbance rejection on a lightly damped plant. Consider the continuous-time SISO plant

$$G(s) = \frac{1}{(s^2 + 2\zeta_1\omega_{n,1}s + \omega_{n,1}^2)(s^2 + 2\zeta_2\omega_{n,2}s + \omega_{n,2}^2)}, \quad (59)$$

where  $\zeta_1 = 0.05$ ,  $\omega_{n,1} = 1$ ,  $\zeta_2 = 0.01$ , and  $\omega_{n,2} = 2$ . The data are sampled with sample period  $T_s = 1$  s. Note that the order of the plant is  $n = 4$ . Let  $u_{\min} = -2$ ,  $u_{\max} = 2$ ,  $\Delta u_{\min} = -2$ ,  $\Delta u_{\max} = 2$ ,  $\theta_0 = [0_{(2\hat{n}-1) \times 1}^T \ 1]^T$ ,  $r_k \equiv 0$ ,  $\lambda = 1$ , and  $P_0 = 10^3 I_{2\hat{n}}$ . No output constraint is considered in this example. At each time step, PCAC solves (37)–(40) with  $\ell = 10$ ,  $\bar{Q} = 50I_{\ell-1}$ ,  $\bar{P} = 50$ , and  $R = 0.1I_\ell$ . A strictly proper model is used for identification in PCAC. Let  $v_k$  be a zero-mean, Gaussian white noise sequence with a standard deviation of 0.005.

Figure 13 shows harmonic disturbance rejection, and Figure 14 shows broadband disturbance rejection using PCAC with  $\hat{n} = n = 4$ ,  $\hat{n} = 5$ , and  $\hat{n} = 6$ . The matched continuous-time harmonic disturbance is given by

$$d(t) = A_d \sin(\omega_d t), \quad (60)$$

where  $A_d = 1$  and  $\omega_d = \pi/15$ . The discrete-time matched broadband disturbance is given by  $d_k$ , where  $d_k$  is a zero-mean, Gaussian white noise sequence with a standard deviation of 0.5. Figures 13(a) and 14(a) consider zero initial conditions for (59), and Figures 13(b) and 14(b) consider nonzero initial conditions, where  $x(0) = [10 \ -5 \ -8 \ 300]^T$  is used as the initial state of the realization

$$\dot{x} = \begin{bmatrix} -0.14 & -2.5 & -0.2 & -2 \\ 2 & 0 & 0 & 0 \\ 0 & 1 & 0 & 0 \\ 0 & 0 & 1 & 0 \end{bmatrix} x + \begin{bmatrix} 0.5 \\ 0 \\ 0 \\ 0 \end{bmatrix} (u + d), \quad (61)$$

$$y = [0 \ 0 \ 0 \ 1]x. \quad (62)$$

Figures 13 and 14 show that, for the asymptotically stable lightly damped plant (59), PCAC rejects harmonic and broadband disturbances. Note that, in the presence of a harmonic disturbance, a pole-zero cancellation occurs at the frequency of the harmonic disturbance, which serves as an implicit internal model of the unknown disturbance. This pole-zero cancellation indicates exogeneity within the closed-loop identification, where RLS captures the frequency and amplitude of the harmonic disturbance to predict and cancel the harmonic disturbance for receding-horizon optimization. Note that this pole-zero cancellation requires that  $\hat{n} \geq n + 2\omega_d$ , where  $\omega_d$  is the number of pure harmonic tones in the disturbance  $d_k$ . For broadband disturbances, as the order of the model increases, the frequency response of the identified model becomes more accurate, thus manifesting exogeneity.  $\diamond$

#### Example 5: A Continuous-Time Unstable Plant

The goal of this example is to investigate PCAC's ability to stabilize an unstable sampled-data plant with a rigid-body mode as well as enforce output and control constraints. Additionally, this example investigates the effect of the constraint slack weight  $S$ . Consider the continuous-time SISO plant

$$G(s) = \frac{1}{s^2(s^2 + 2\zeta s + 1)}. \quad (63)$$

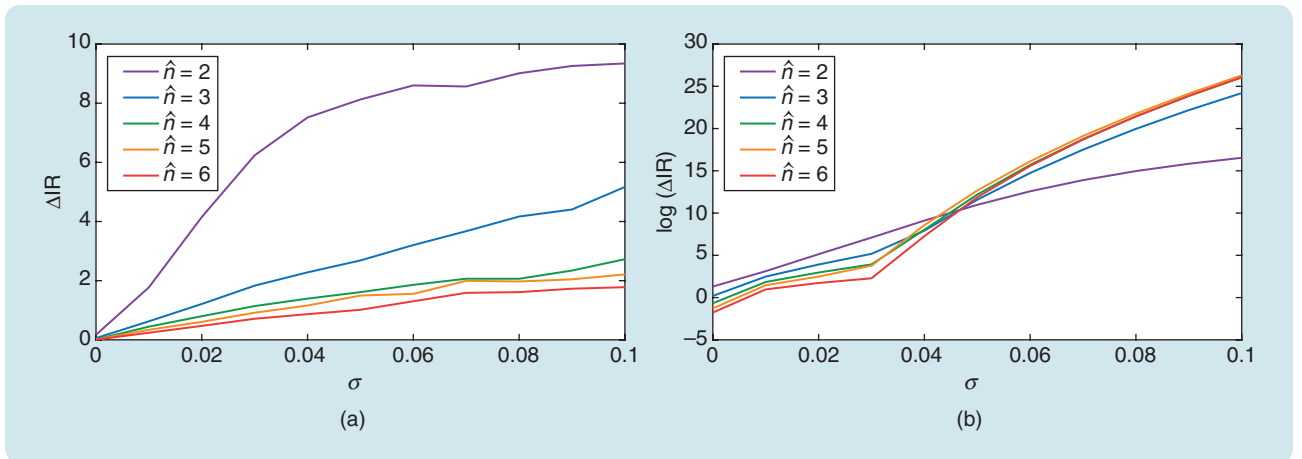


**FIGURE 11** Example 2: Accuracy of the identified model versus the standard deviation  $\sigma$  of the sensor noise for the discrete-time unstable nonminimum-phase single-input, single-output plant (53) with  $r_k \equiv 1$  and with the controllers given by predictive cost adaptive control (PCAC) and linear quadratic Gaussian (LQG) with an integrator. The model accuracy is determined by  $\Delta IR$  at  $k = 140$  averaged over 100 simulations. PCAC uses a strictly proper finite-impulse response initial model, and LQG with an integrator uses (53) to compute the control gain with output and control weights  $Q = 2$  and  $R = 1$ , respectively. (a) PCAC. For each  $\sigma$ , larger values of  $\hat{n}$  yield smaller values of  $\Delta IR$ . Therefore, for each sensor-noise level, the identified model is more accurate for larger values of  $\hat{n}$ . (b) LQG with an integrator. For each  $\hat{n}$ , larger values of  $\sigma$  yield larger values of  $\Delta IR$ . Note that, unlike (a), for all  $\sigma \geq 0.05$ , an increase in the model order  $\hat{n}$  results in a less accurate model. In addition, for each value of  $\hat{n}$ , the models in (b) are less accurate than those in (a).  $\Delta IR$ : the  $L_2$ -norm difference between the 30-step impulse response of the plant and model.

The data are sampled with sample period  $T_s = 1$  s. Let  $u_{\min} = -10$ ,  $u_{\max} = 10$ ,  $\Delta u_{\min} = -5$ ,  $\Delta u_{\max} = 5$ ,  $\lambda = 1$ ,  $P_0 = 10^3 I_{2\hat{n}}$ ,  $\ell = 20$ ,  $\tilde{Q} = 40I_{\ell-1}$ ,  $\tilde{P} = 40$ , and  $R = 10I_{\ell}$ . PCAC is initialized with the strictly proper FIR model  $\theta_0 = [0_{(2\hat{n}-1) \times 1}^T \ 1]^T$ , and  $v_k$  is a zero-mean, Gaussian white sequence with a standard deviation of 0.001. Let the output constraint be given by (5), where  $C = [1 \ -1]^T$ , and  $\mathcal{D} = [-20 \ -20]^T$ . A realization of (63) is given by

$$\dot{x} = \begin{bmatrix} -2\zeta & -1 & 0 & 0 \\ 1 & 0 & 0 & 0 \\ 0 & 1 & 0 & 0 \\ 0 & 0 & 1 & 0 \end{bmatrix} x + \begin{bmatrix} 1 \\ 0 \\ 0 \\ 0 \end{bmatrix} u, \quad (64)$$

$$y = [0 \ 0 \ 0 \ 1]x. \quad (65)$$

Denote the  $i$ th component of  $u_k$ ,  $\Delta u_{\max}$ ,  $\Delta u_{\min}$ , and  $u_{1|k}$ , by  $u_{k,i}$ ,  $\Delta u_{\max,i}$ ,  $\Delta u_{\min,i}$ , and  $u_{1|k,i}$ , respectively. In this example, for each  $i = 1, \dots, m$ , the saturation

$$u_{k+1,i} = \begin{cases} \min(\max(u_{k,i} + \Delta u_{\max,i}, u_{\min,i}), u_{\max,i}), & u_{1|k,i} - u_{k,i} > \Delta u_{\max,i} \\ \min(\max(u_{k,i} + \Delta u_{\min,i}, u_{\min,i}), u_{\max,i}), & u_{1|k,i} - u_{k,i} < \Delta u_{\min,i} \\ \min(\max(u_{1|k,i}, u_{\min,i}), u_{\max,i}), & \text{otherwise} \end{cases} \quad (66)$$

is applied.

Figure 15 shows the response of PCAC for various values of the constraint relaxation weight  $S$ . Figure 15(a) shows the response of PCAC using (37)–(40) as well as from (41)–(45)

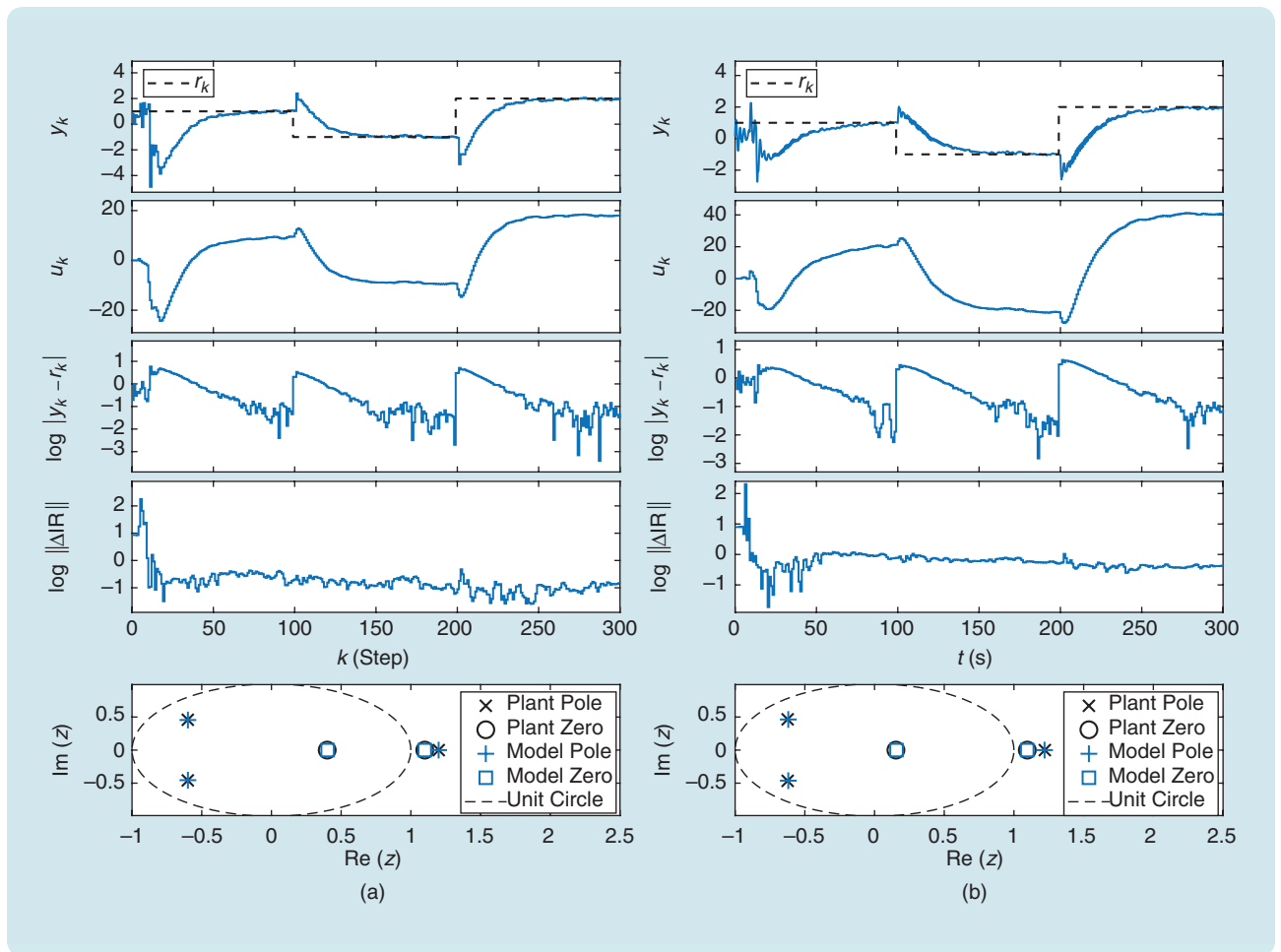


**FIGURE 12** Example 3: Command following for the unstantly stabilizable single-input, single-output plants (54) and (56) using  $\hat{n} = n = 3$  and the three-step command (55). (a) For the discrete-time plant (54), the output  $y_k$  approaches each step command with a decreasing command-following error. The bottom-most plot compares the poles and zeros of the identified model at  $k = 300$  to the poles and zeros of the plant. It was observed (not shown) that the response time was larger than 100 steps for  $32 \leq \ell \leq 40$ , and PCAC was unable to follow the step commands for  $\ell \leq 31$ . For  $\ell > 85$ , it was observed (not shown) that the output diverged. (b) For the continuous-time plant (56), the output  $y(t)$  approaches each step command with a decreasing command-following error. The bottom-most plot compares the poles and zeros of the identified model at  $t = 300$  s to the poles and zeros of the exact discretization of the continuous-time plant (56). Note that the discretized plant is unstantly stabilizable.  $\Delta R$ : the  $L_2$ -norm difference between the 30-step impulse response of the plant and model.

with  $\hat{n} = n = 4$ ,  $\zeta = 0.7$ ,  $x(0) = [1 \ -3 \ 2 \ 0.5]^T$ , and the three-step command

$$r_k = \begin{cases} 0, & 0 \leq k < 50, \\ 19, & 50 \leq k < 80, \\ -25, & k \geq 80. \end{cases} \quad (67)$$

Figure 15(b) shows the response of PCAC using (41)–(45) with  $\hat{n} = 6 > n = 4$ ,  $\zeta = 0.01$ ,  $x(0) = [10 \ -5 \ 8 \ 3]^T$ , and the three-step command

$$r_k = \begin{cases} 0, & 0 \leq k < 120, \\ 19, & 120 \leq k < 150, \\ -25, & k \geq 150. \end{cases} \quad (68)$$

Figure 15 shows that, for the unstable plant (63), PCAC stabilizes the plant, and the output approaches the feasible commands. Note that the nonzero constraint relaxation weight reduces the overall constraint violation, especially in cases where the combination of the commands and constraints is

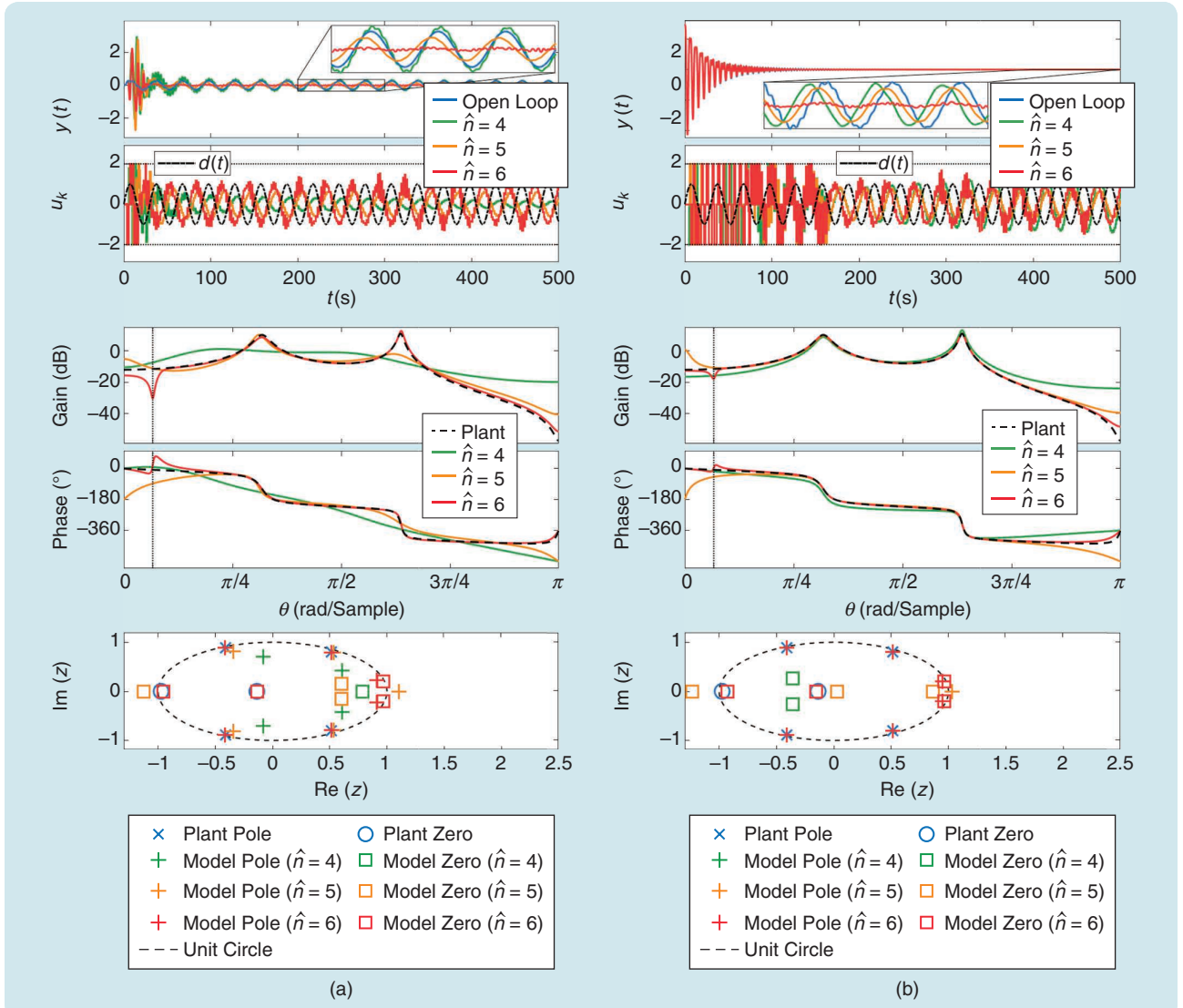


**FIGURE 13** Example 4: Matched disturbance rejection for the continuous-time asymptotically stable single-input, single-output plant (59) and harmonic disturbance (60) with  $\hat{n} = n = 4$ ,  $\hat{n} = 5$ , and  $\hat{n} = 6$ . (a) Zero initial conditions. Note that larger values of  $\hat{n}$  yield a better performance and that  $u_k$  approximately cancels  $d(t)$  for  $\hat{n} = 6$ . Furthermore, larger values of  $\hat{n}$  yield a more accurate frequency response of the identified models at  $t = 500$  s. For  $\hat{n} = 6$ , the identified model has an approximate pole-zero cancellation at the disturbance frequency  $\theta_d = \pi/15$  rad/sample, which is denoted by the vertical dash-dotted line; the spurious pole in the identified model allows receding-horizon optimization to predict the future harmonic response of the plant, which facilitates the optimization of the future control inputs. This pole-zero cancellation serves as an implicit internal model of the unknown disturbance. The bottom-most plot compares the poles and zeros of the identified model at  $t = 500$  s to the poles and zeros of the exact discretization of the plant. For  $\hat{n} = 6$ , the approximate pole-zero cancellations on the unit circle occur at the frequency  $\theta_d$  of the harmonic disturbance. (b) Nonzero initial conditions  $x(0) = [10 \ -5 \ -8 \ 300]^T$  for the state-space realization (61), (62). Compared to the case of zero initial conditions, the transient response is more pronounced, and the control saturation occurs over a longer interval of time. Moreover, since nonzero initial conditions result in more persistency during the transient, the identified models in (b) are more accurate than those in (a).

**Although PEM and IV are more accurate than RLS/VRF for both open- and closed-loop identification, these methods were found to be less compatible with PCAC than RLS/VRF.**

infeasible. Furthermore, the constraint violation is reduced as the model accuracy improves.  $\diamond$

### LINEAR MULTIPLE-INPUT, MULTIPLE-OUTPUT EXAMPLES

This section considers linear time-invariant MIMO plants with the state-space realization (1) along with

$$\tilde{y} = Cx + Du, \quad (69)$$

$$\tilde{z} = Ex, \quad (70)$$

where  $w(t) \in \mathbb{R}^{l_w}$  is an unmatched disturbance,  $\tilde{y}(t) \in \mathbb{R}^{l_y}$ ,  $\tilde{z}(t) \in \mathbb{R}^{l_z}$ ,  $A \in \mathbb{R}^{l_x \times l_x}$ ,  $B \in \mathbb{R}^{l_x \times m}$ ,  $C \in \mathbb{R}^{l_y \times l_x}$ ,  $D \in \mathbb{R}^{l_y \times m}$ ,  $D_1 \in \mathbb{R}^{l_z \times l_w}$ , and  $E \in \mathbb{R}^{l_z \times l_x}$ . At each time step, PCAC uses the sampled measurement, where  $y_k = [\tilde{y}_k^T \tilde{z}_k^T]^T \in \mathbb{R}^{l_y+l_z}$ , and the tracking output (3) and constrained output (4) are based on  $\tilde{z}_k$ . Note that both  $\tilde{y}_k$  and  $\tilde{z}_k$  are noisy measurements, and  $\tilde{z}_k$  is used to define the performance metric.

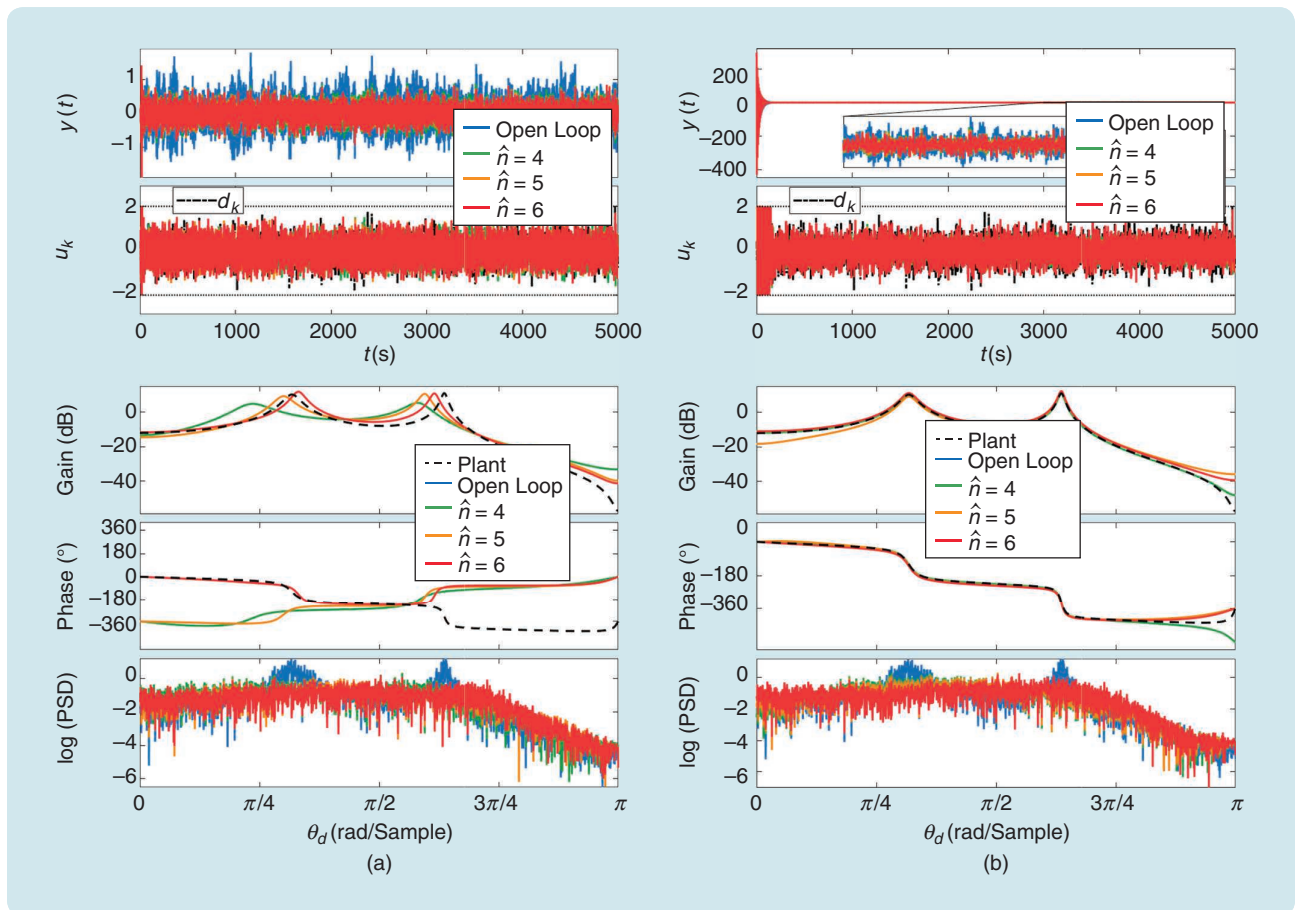


**FIGURE 14** Example 4: Matched disturbance rejection for the continuous-time asymptotically stable single-input, single-output plant (59) and zero-mean, Gaussian white noise sequence  $d_k$  with a standard deviation of 0.5 for  $\hat{n} = n = 4, \hat{n} = 5$ , and  $\hat{n} = 6$ . (a) Zero initial conditions. Note that larger values of  $\hat{n}$  yield more accurate magnitudes of the frequency response of the identified models at  $t = 5000$  s. The bottom-most plot shows that, for all  $\hat{n}$ , predictive cost adaptive control (PCAC) reduces the two peaks of the open-loop power spectral density (PSD) of  $y_k$ , which indicates that PCAC rejects the broadband disturbance  $d_k$ . (b) Nonzero initial conditions  $x(0) = [10 \ -5 \ -8 \ 300]^T$  for the state-space realization (61) and (62). As in (a), the bottom-most plot shows that, for all  $\hat{n}$ , PCAC reduces the two peaks of the open-loop PSD of  $y_k$ . Note that, for all  $\hat{n}$ , the frequency responses of the identified models at  $t = 5000$  s are more accurate in (b) than in (a) due to the nonzero initial conditions.

**Example 6: An Asymptotically Stable Plant With Nonminimum-Phase Transmission Zeros and Nonminimum-Phase Channel Zeros**

The goal of this example is to investigate the applicability of PCAC MIMO plants. Consider the continuous-time plant MIMO (1)–(70), where

$$A = \begin{bmatrix} 0 & 1 & 0 & 0 & 0 & 0 \\ -1.4 & -0.06 & 0.4 & 0.05 & 0 & 0 \\ 0 & 0 & 0 & 1 & 0 & 0 \\ 0.8 & 0.1 & -1 & -0.16 & 0.2 & 0.06 \\ 0 & 0 & 0 & 0 & 0 & 1 \\ 0 & 0 & 1 & 0.3 & -1 & -0.3 \end{bmatrix}, B = \begin{bmatrix} 0 & 0 \\ 1 & 0 \\ 0 & 0 \\ 0 & 2 \\ 0 & 0 \\ 0 & 0 \end{bmatrix}, \quad (71)$$

$$C = \begin{bmatrix} 0 & 0 & -3.1 & 3.3 & 0 & 0 \\ 0 & 0 & 0 & 0 & 0.31 & -0.33 \end{bmatrix}, D = 0_{2 \times 2}, \quad (72)$$

$$D_1 = \begin{bmatrix} -0.1 & 0 \\ 0 & 0 \\ 0 & 0 \\ 0 & 0 \\ 0 & 0 \\ 0 & -0.5 \end{bmatrix}, E = [2 \ -2.1 \ 0 \ 0 \ 0 \ 0]. \quad (73)$$

The transmission zeros (TZs) and channel zeros (CZs) of (71)–(73) are shown in Figure 16. The data are sampled with sample period  $T_s = 0.5$  s. Let  $u_{\min} = [-2 \ -1]^T$ ,  $u_{\max} = [2 \ 1]^T$ ,  $\Delta u_{\min} = [-1 \ -0.5]^T$ ,  $\Delta u_{\max} = [1 \ 0.5]^T$ ,  $\lambda = 1$ ,  $P_0 = 10^3 I_{2i}$ ,  $\ell = 10$ ,  $\bar{Q} = 40I_{\ell-1}$ ,  $\bar{P} = 40$ ,  $R = \begin{bmatrix} 10 & 0 \\ 0 & 10 \end{bmatrix} \otimes I_{\ell}$ , and  $r_k \equiv 0$ . Let  $v_k$  be a zero-mean, Gaussian white noise sequence with a standard deviation of 0.02. The plant is initialized with

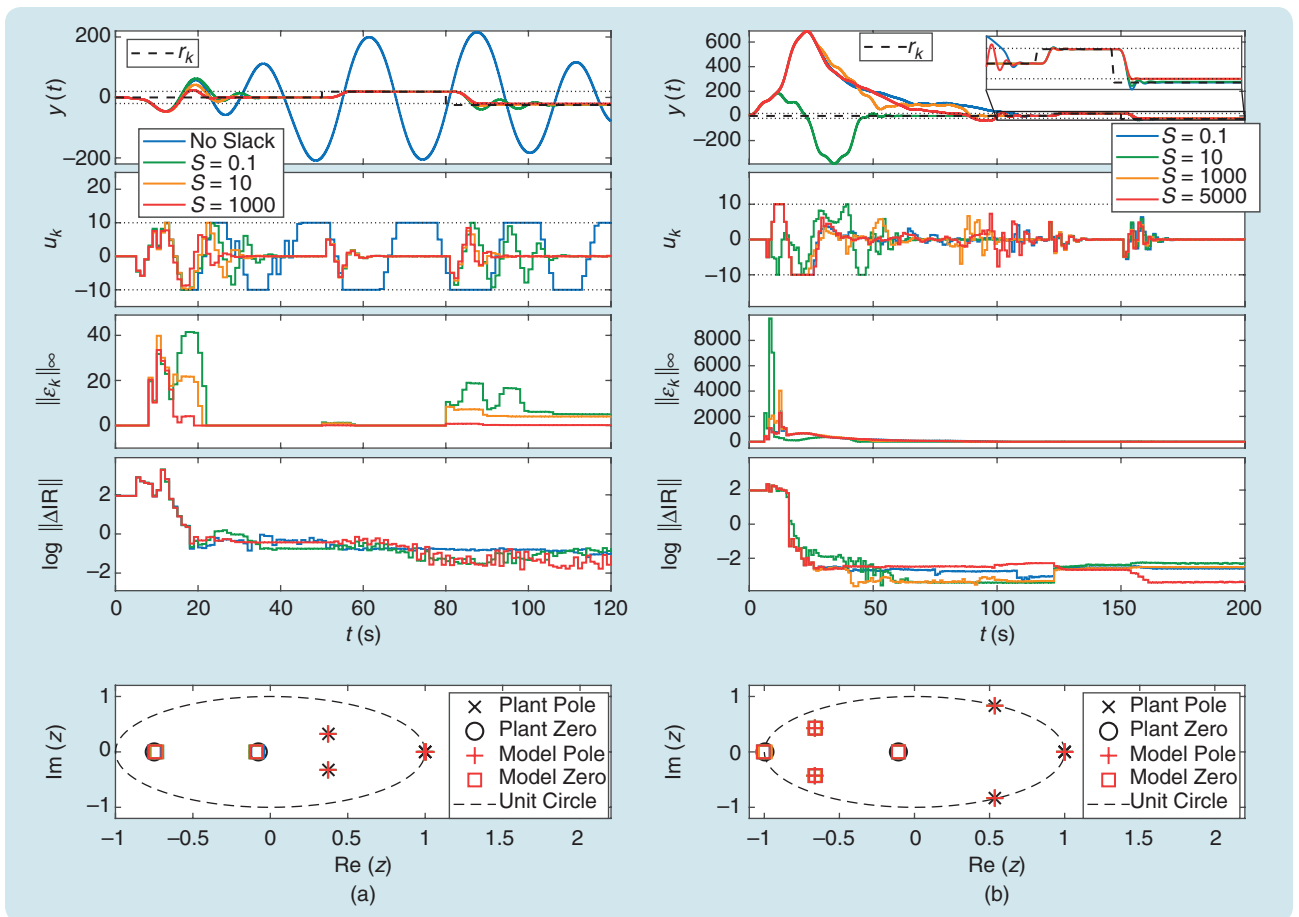


**FIGURE 15** Example 5: Command following with the output constraint  $-20 \leq y_k \leq 20$  and continuous-time unstable single-input, single-output plant (63) for various values of  $S$ . (a) Predictive cost adaptive control (PCAC) is applied using (37)–(40) and (41)–(45) with  $\hat{n} = n = 4$ ,  $\zeta = 0.7$ ,  $x(0) = [1 \ -3 \ 2 \ 0.5]^T$ , and the three-step command (67). At  $t = 9$  s, (37)–(40) become infeasible, and the three-step command cannot be followed. In contrast, with (41)–(45),  $y(t)$  approaches the first two step commands, and the slack is activated at  $t = 8$  s,  $t = 50$  s, and  $t = 80$  s, as can be seen in the third plot. Since the last step command is not achievable,  $y(t)$  moves further away from the command as  $S$  increases, where the command-following error at  $t = 120$  s is approximately 0.02 for  $S = 0.1$ , 1.00 for  $S = 10$ , and 4.81 for  $S = 1000$ . Furthermore, note that the overshoot at  $t = 19$  s violates the output constraint due to the poor initial model and nonzero initial condition. The distance between  $y(t)$  and the constraint at  $t = 19$  s for  $S = 0.1$  is 41.47, which is reduced by 47% for  $S = 10$  and 89% for  $S = 1000$ . (b) PCAC is applied using (41)–(45) with  $\hat{n} = 6 > n = 4$ ,  $\zeta = 0.01$ ,  $x(0) = [10 \ -5 \ 8 \ 3]^T$ , and the three-step command (68). Compared to (a), note that, for all  $S$ , the output-constraint violation is more severe during the first transient. However, as the model becomes more accurate,  $y(t)$  approaches the first and second step commands, where the constraint is enforced after  $t = 106$  s. For the third step command, as in (a),  $y(t)$  moves away from the step command as  $S$  increases.  $\Delta IR$ : the  $L_2$ -norm difference between the 30-step impulse response of the plant and model.

$x(0) = [1 \ -3 \ 5 \ 0.5 \ 2 \ -1]^T$ , and PCAC uses (37)–(40) with the strictly proper FIR initial model  $\theta_0 = [0_{\hat{n}p(m+p) \times 1}^T \ 1_{mp \times 1}]^T$ . No output constraint is considered in this example, and the tracking output  $y_{t,k}$  is given by (3) with  $C_t = [0 \ 0 \ 1]$ ; that is,  $y_{t,k} = \tilde{z}_k$ .

Figure 17 shows broadband disturbance rejection for  $\hat{n} = 3$ ,  $\hat{n} = 4$ , and  $\hat{n} = 6$ . The discrete-time unmatched broadband disturbance is given by the random vector  $w_k = [w_{1,k} \ w_{2,k}]^T \in \mathbb{R}^2$ , where the components  $w_{1,k}$  and  $w_{2,k}$  are zero-mean, Gaussian white noise sequences with standard deviations of 1.7 and 2.5, respectively. Figure 17 shows that, for the MIMO plant (71)–(73) with NMP TZ and NMP CZ, PCAC rejects an unmatched broadband disturbance.  $\diamond$

**Example 7: An Unstable Plant With Nonminimum-Phase Transmission Zeros and Nonminimum-Phase Channel Zeros**  
The goal of this example is to investigate the ability of PCAC to stabilize MIMO plants while enforcing output constraints. Consider the continuous-time MIMO plant (1)–(70), where  $B$  is given by (71),  $C$  and  $D$  are given by (72),  $D_1 = 0_{6 \times 2}$ , and

$$A = \begin{bmatrix} 0 & 1 & 0 & 0 & 0 & 0 \\ -1.4 & -0.06 & 0.4 & 0.05 & 0 & 0 \\ 0 & 0 & 0 & 1 & 0 & 0 \\ 0.8 & 0.1 & -1 & -0.04 & 0.2 & -0.06 \\ 0 & 0 & 0 & 0 & 0 & 1 \\ 0 & 0 & 1 & -0.3 & -1 & 0.3 \end{bmatrix}, \quad (74)$$

$$E = \begin{bmatrix} 2 & -2.1 & 0 & 0 & 0 & 0 \\ 0 & 1 & 0 & 0 & 0 & -1.1 \end{bmatrix}.$$

The TZ and CZ of (74) are shown in Figure 18. The data are sampled with sample period  $T_s = 0.5$  s. Let  $u_{\min} = [-15 \ -5]^T$ ,  $u_{\max} = [15 \ 5]^T$ ,  $\Delta u_{\min} = [-5 \ -2]^T$ ,  $\Delta u_{\max} = [5 \ 2]^T$ ,  $\lambda = 1$ ,  $P_0 = 10^3 I_{2\hat{n}}$ ,  $\ell = 40$ ,  $\bar{Q} = 40I_{\ell-1}$ ,  $\bar{P} = 40$ , and  $R = \begin{bmatrix} 10 & 0 \\ 0 & 10 \end{bmatrix} \otimes I_\ell$ . Let  $v_k$  be a zero-mean, Gaussian white noise sequence with a standard deviation of 0.02. The plant is initialized with  $x(0) = [2 \ -3.3 \ 4 \ -2.6 \ 2 \ -1.3]^T$ , and PCAC uses (41)–(45) with the strictly proper FIR initial model  $\theta_0 = [0_{(\hat{n}(m+p)p - mp) \times 1}^T \ 1_{mp \times 1}]^T$ . The tracking output  $y_{t,k}$  is given by (3) with  $C_t = [1 \ 0]$ , and the constrained output is given by (4) with  $C_c = [0 \ 1]$ ; that is,  $y_{t,k} = \tilde{z}_{1,k}$ , and  $y_c = \tilde{z}_{2,k}$ . The output constraint is given by (5), where  $\mathcal{C} = [1 \ -1]^T$ , and  $\mathcal{D} = [-10 \ -10]^T$ .

Figure 19 shows the response of PCAC for  $\hat{n} = 2$  and various values of  $S$  using the three-step command

$$r_k = \begin{cases} 0, & 0 \leq k < 40, \\ 10, & 40 \leq k < 80, \\ -20, & k \geq 80. \end{cases} \quad (75)$$

Figure 18 shows that, for the unstable MIMO plant (71), (72), and (74) with NMP TZ and NMP CZ, PCAC stabilizes the plant while asymptotically satisfying the output constraints, and the output approaches the step commands.  $\diamond$

## LINEAR TIME-VARYING EXAMPLES

This section considers linear time-varying SISO plants, where  $y_{t,k} = y_{c,k} = y_k$ .

### Example 8: Abrupt Change From an Asymptotically Stable Plant to an Unstable Nonminimum-Phase Plant

The goal of this example is to investigate the applicability of PCAC with VRF on time-varying plants. Consider a discrete-time asymptotically stable SISO plant (46) that abruptly changes at step  $k_c$  to a discrete-time unstable NMP SISO plant (53). Note that the orders of both plants are  $n = 2$  with relative degree one.

Let  $u_{\min} = -50$ ,  $u_{\max} = 50$ ,  $\Delta u_{\min} = -25$ ,  $\Delta u_{\max} = 25$ ,  $\ell = 20$ ,  $\bar{Q} = 2I_{\ell-1}$ ,  $\bar{P} = 5$ ,  $R = I_\ell$ ,  $\hat{n} = n = 2$ , and  $P_0 = 10^3 I_{2\hat{n}}$ . No output constraint is considered in this example. The plant is initialized with  $y_{-1} = -0.2$ ,  $y_{-2} = 0.4$ , and  $u_{-1} = u_{-2} = 0$ . PCAC uses the strictly proper FIR initial model  $\theta_0 = [0_{1 \times 3} \ 1]^T$  and uses (37)–(40) with the measurement  $y_k$ . Let  $v_k = 0$ .

Figure 20 shows the response of PCAC for  $r_k \equiv 1$  using CRF with  $\lambda = 1$  and VRF (21) with  $\eta = 0.9$ ,  $\tau_n = 5$ , and  $\tau_d = 10$  for  $k_c = 30$ ,  $k_c = 200$ ,  $k_c = 400$ , and  $k_c = 600$ . Figure 20(a) shows that, in the absence of forgetting, that is,  $\lambda = 1$ , reidentification of the plant after the abrupt change is poor, and the output does not approach the step command. In contrast, Figure 20(b)

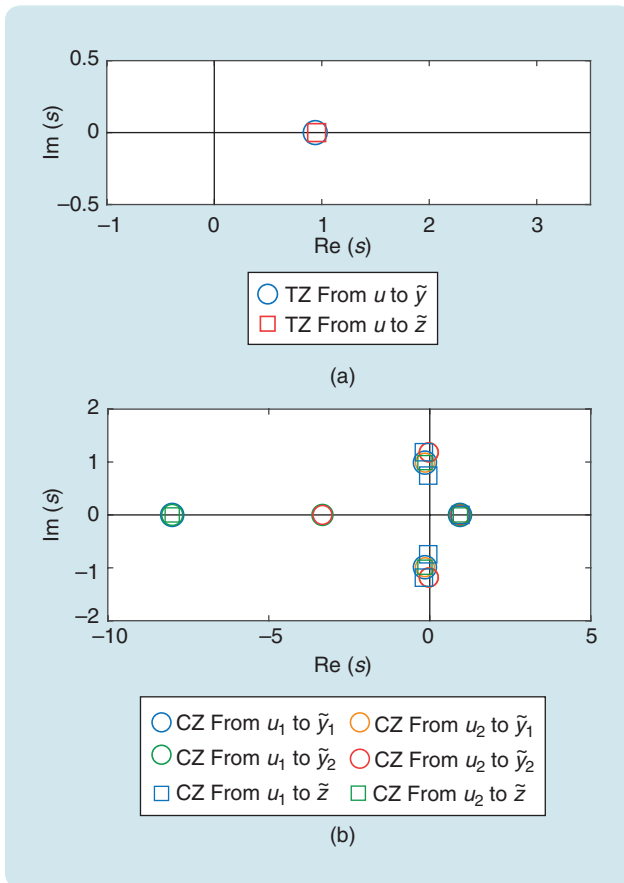


**FIGURE 16** Example 6: Transmission zeros (TZs) and channel zeros (CZs) of the continuous-time asymptotically stable multiple-input, multiple-output plant (71)–(73). (a) The transfer function from  $u$  to  $[\tilde{y}^T \ \tilde{z}^T]^T$  has two nonminimum-phase (NMP) TZs at approximately  $z_t = 0.94$ . (b) Each transfer function has one NMP CZ at approximately 0.94.

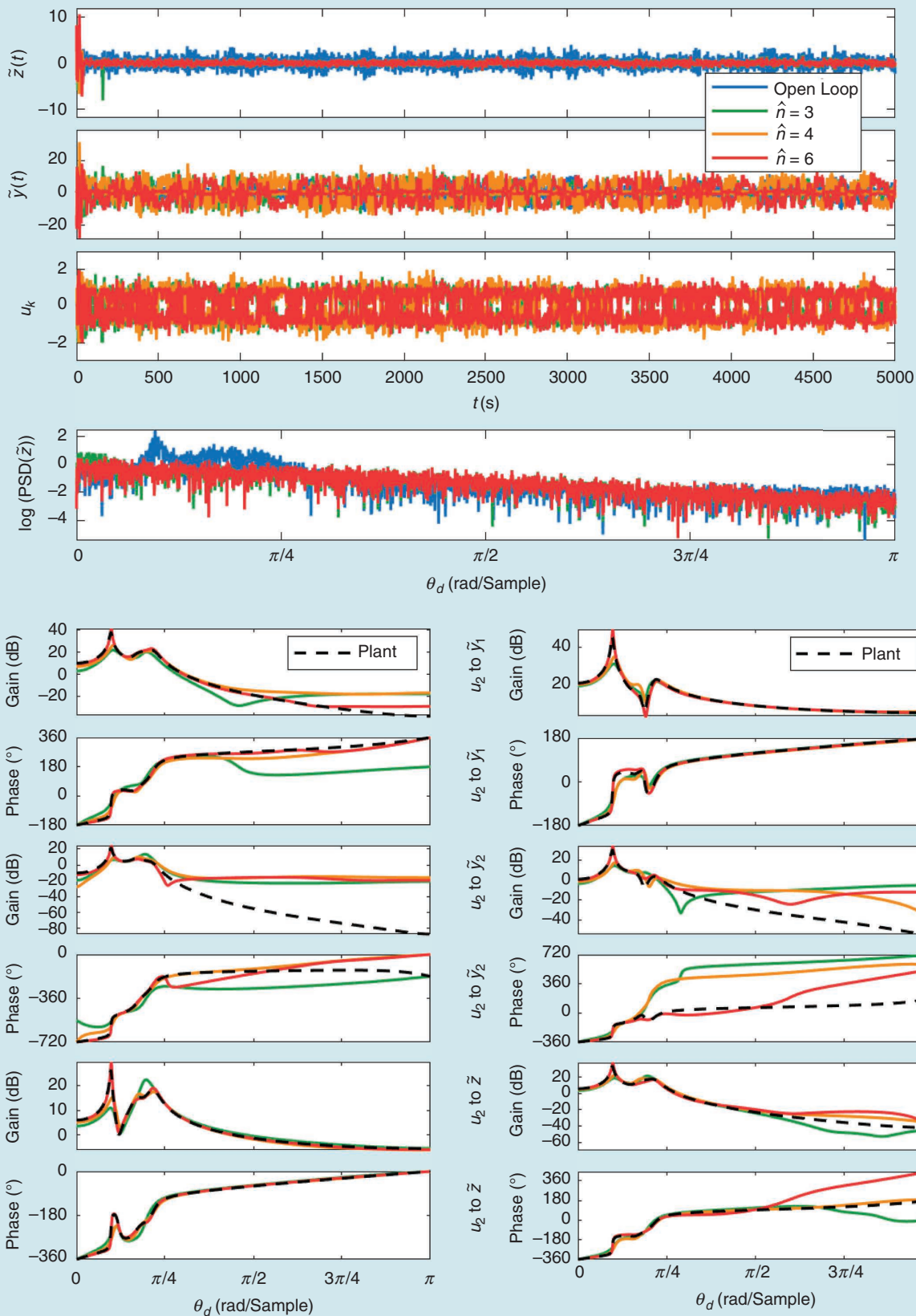


**FIGURE 17** Example 6: Unmatched broadband disturbance rejection for the continuous-time asymptotically stable multiple-input, multiple-output plant (71)–(73) with a nonminimum-phase (NMP) transmission zero and an NMP channel zero for  $\hat{n} = 3$ ,  $\hat{n} = 4$ , and  $\hat{n} = 6$  using the discrete-time broadband disturbance  $w_k = [w_{1,k} \ w_{2,k}]^T \in \mathbb{R}^2$ , where  $w_{1,k}$  and  $w_{2,k}$  are zero-mean, Gaussian white noise sequences with 1.7 and 2.5, respectively. Note that, for all  $\hat{n}$ , the magnitude of the open-loop power spectral density (PSD) of  $\tilde{z}$  in the range  $\pi/16 \leq \theta_d \leq \pi/4$  is reduced, which indicates suppression of the broadband disturbance  $w_k$ . For all six channels, namely, from  $u_1$  and  $u_2$  to  $\tilde{y}_1$ ,  $\tilde{y}_2$ , and  $\tilde{z}$ , the 12 bottom-most plots compare the frequency response of the identified model at  $t = 5000$  s to the frequency response of the plant. As in Example 4, this example shows that a larger model order  $\hat{n}$  yields more accurate estimates of the plant dynamics.

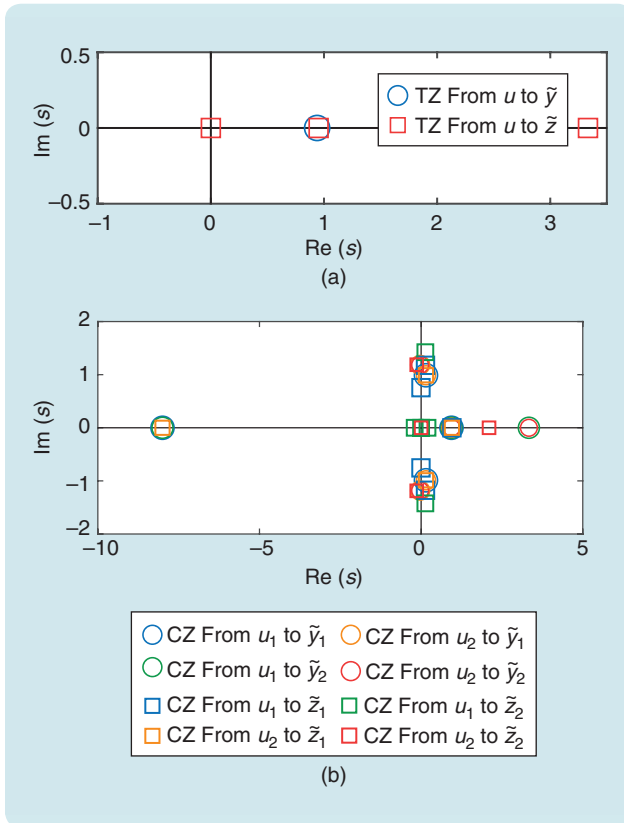


**FIGURE 18** Example 7: The transmission zero (TZ) and channel zero (CZ) of the continuous-time unstable multiple-input, multiple-output plant (74). (a) The transfer function from  $u$  to  $[\tilde{y} \tilde{z}]^T$  has four nonminimum-phase (NMP) TZs at approximately 0.00, 0.94, and 3.33. (b) The eight transfer functions have 21 NMP CZs at approximately 0.00,  $0.13 \pm 1.42j$ ,  $0.14 \pm 1.18j$ ,  $0.15 \pm 0.99j$ , 0.19, 0.95, 2.10, and 3.33.

shows that, with VRF, reidentification of the plant after the abrupt change is better compared to Figure 20(a), and, thus, the output approaches the step commands.  $\diamond$

### Example 9: Abrupt Change From an Asymptotically Stable Plant to an Unstable Nonminimum-Phase Plant With Sensor Noise

The goal of this example is to investigate the effect of zero-mean, Gaussian white sensor noise on VRF. This example uses the same setup as Example 8 except that PCAC now uses noisy measurements with the command profile

$$r_k = \begin{cases} 20, & 0 \leq k < 100, \\ -20, & 100 \leq k < 200, \\ 3, & 200 \leq k < 400, \\ -50, & k \geq 400. \end{cases} \quad (76)$$

Figure 21 shows the response of PCAC for two different levels of sensor noise using  $k_c = 300$  and VRF (21) with  $\eta = 0.5$ ,  $\tau_d = 5\tau_n$ , and various values of  $\tau_n$ . As shown in Figure 21(a) and (b), as  $\tau_n$  increases, the duration during which forgetting is active increases. Hence, as  $\tau_n$  increases, reidentification becomes slower and, for large values of  $\tau_n$ , the output does not approach the command. Note that, as  $\tau_n$  increases, the VRF  $\lambda_k$  becomes less sensitive to sensor noise.

Note that the speed of convergence of the coefficients after the abrupt change determines whether or not the output approaches the command. In particular, with a large choice of  $\tau_n$ , the reconvergence of the model coefficients is slow, which yields a divergence of the output. Furthermore, in the presence of zero-mean, Gaussian white sensor noise, where  $\tau_d = 5\tau_n$ , increasing the value of  $\tau_n$  reduces the activation of forgetting due to sensor noise.  $\diamond$

## Guidelines for Selecting Hyperparameters

This is a list of the hyperparameters that need to be selected for predictive cost adaptive control as well as heuristic guidelines on how to select them.

- **Identification model order  $\hat{n}$ :** Choose  $\hat{n}$  to be greater than or equal to the dimension of the unstable subspace of the plant. Add +2 for each harmonic disturbance.
- **Initial identification covariance  $P_0$ :** Typically, choose  $P_0 = \alpha I_{\hat{n}p(m+p)+mp}$ , where  $10^{-4} \leq \alpha \leq 10^4$ . Larger values of  $\alpha$  yield more aggressive identification and may lead to more severe transients in the response.
- **Initial identification coefficient vector  $\theta_0$ :** Use the best prior estimate of the plant coefficients when available; otherwise, set  $\theta_0 = 0.01 \cdot \mathbf{1}_{[\hat{n}p(m+p)+mp] \times 1}$ .
- **Constant forgetting factor  $\lambda$ :** Typically, choose  $0.95 \leq \lambda \leq 1$ . Choose  $\lambda = 1$  when persistency is lacking. Not relevant when using variable-rate forgetting (VRF).
- **VRF parameters  $\tau_n, \tau_d$ :**  $\tau_d = 5\tau_n$ , where  $1 \leq \tau_n \leq 100$ . Smaller  $\tau_n$  yields identification that reacts quickly to

changes but is more sensitive to sensor noise. On the other hand, larger  $\tau_n$  yields identification that reacts slowly to changes but is less sensitive to sensor noise.

- **VRF parameter  $\eta$ :**  $0.001 \leq \eta \leq 1$ . Larger values of  $\eta$  yield more aggressive forgetting in response to changes.
- **Prediction horizon  $\ell$ :** Select the prediction horizon  $\ell$  so that  $\ell T_s$  is greater than the settling time of the plant. For unstable plants, excessively large values of  $\ell$  may lead to divergence.
- **Cost-to-go output weight  $\bar{Q}$ :**  $\alpha I_{(\ell-1)p}, \alpha > 0$ .
- **Terminal output weight  $\bar{P}$ :**  $\alpha I_p, \alpha > 0$ .
- **Control move-size weight  $R$ :**  $\alpha I_m, \alpha \geq 0$ .
- **Constraint relaxation weight  $S$ :**  $\alpha I_{m \times c}, \alpha \geq 0$ . Choose non-zero  $\alpha$  when infeasible command and constraints are expected.
- **Control magnitude constraints  $u_{min}, u_{max}$ :** Select these values to reflect actuator magnitude constraints.
- **Control move-size constraints  $\Delta u_{min}, \Delta u_{max}$ :** Select these values to reflect actuator move-size constraints.

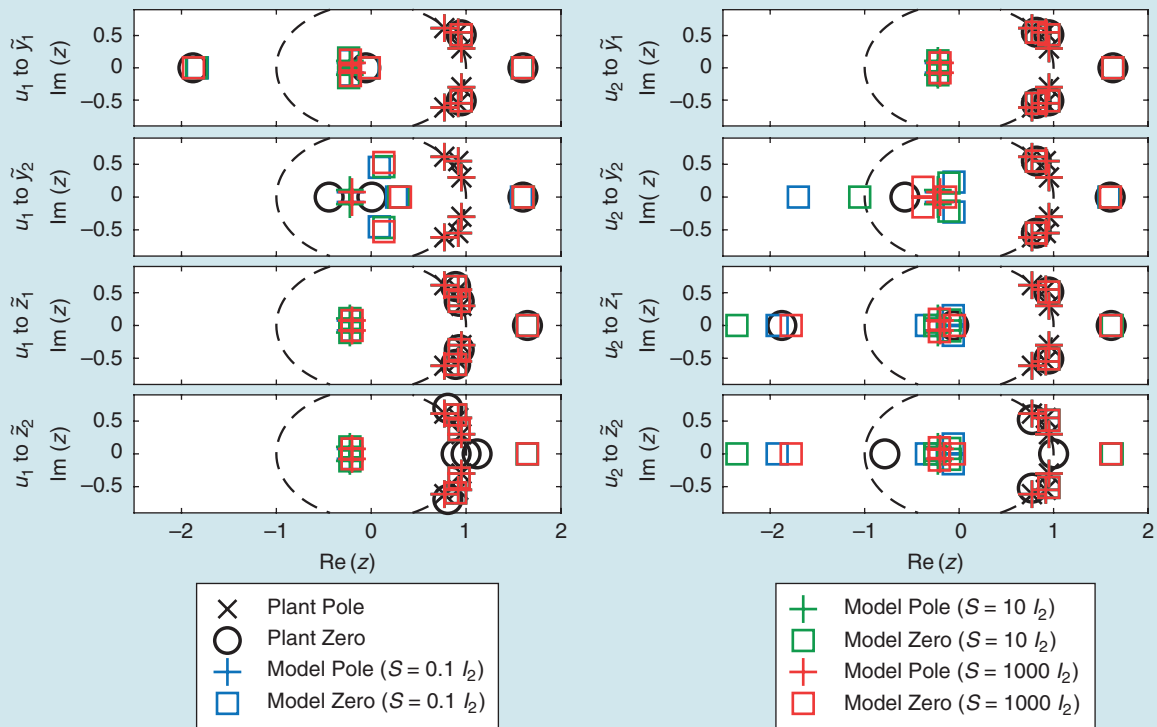
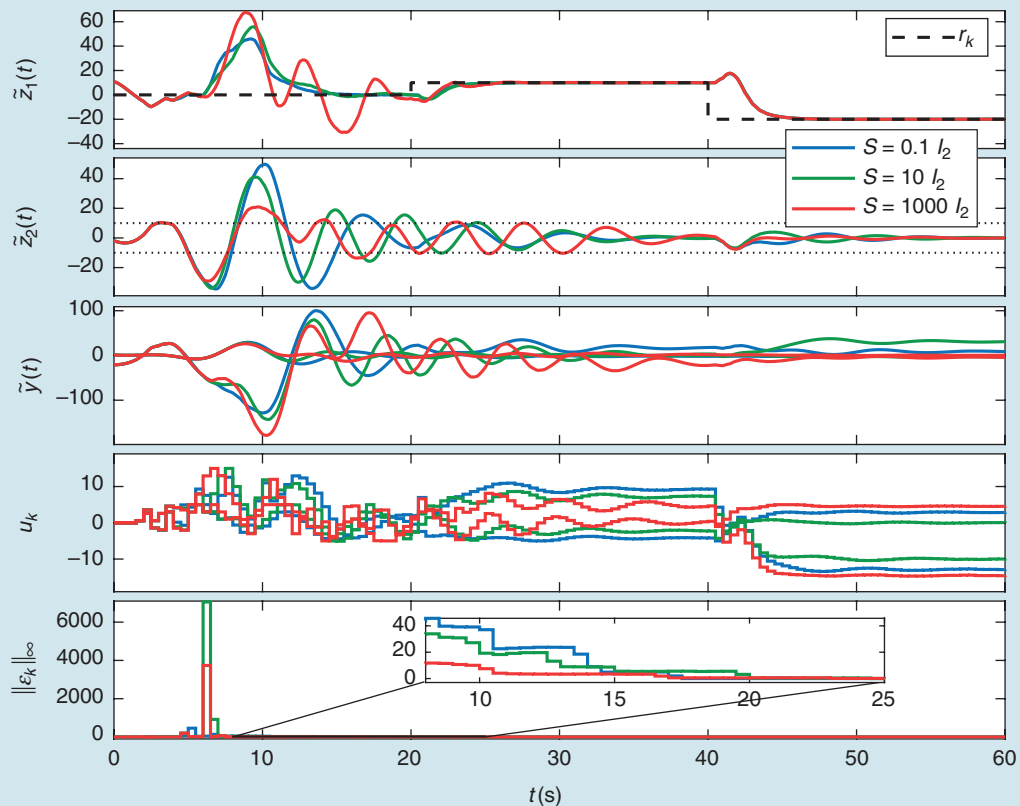


**FIGURE 19** Example 7: Command following for the continuous-time unstable multiple-input, multiple-output plant (74) with the nonminimum-phase (NMP) transmission zero and NMP channel zero for  $\hat{n} = 2$  and various values of  $S$  using the three-step command (75). For each  $S$ , the tracking output approaches the three-step command. Note that, as  $S$  increases, the output-constraint violation becomes less severe. Due to the poor initial model, the output constraint is relaxed by the slack  $\epsilon_k$  until  $t = 20$  s. For all  $t \geq 20$  s, note that, for each  $S$ , as the model becomes more accurate and  $\tilde{z}_1(t)$  approaches zero, the output constraint is enforced. The eight bottom-most plots compare the poles and zeros of the identified model at  $t = 60$  s to the poles and zeros of the plant.

**Example 10: Abrupt Change From an Asymptotically Stable Plant to an Unstable Plant With Sensor Noise and Output Constraints**

The goal of this example is to demonstrate PCAC with VRF with output constraints. Consider a continuous-time asymptotically stable SISO plant

$$G(s) = \frac{4}{s^2 + 0.1s + 0.3} \quad (77)$$

that abruptly changes at time 300 s to a continuous-time unstable SISO plant (63) with  $\zeta = 0.01$ . Note that the order of (63) is  $n = 4$ , and the order of (77) is  $n = 2$ . A realization of (77) is given by

$$\dot{x} = \begin{bmatrix} -0.1 & -0.6 \\ 0.5 & 0 \end{bmatrix} x + \begin{bmatrix} 4 \\ 0 \end{bmatrix} u, \quad (78)$$

$$y = [0 \ 2]x, \quad (79)$$

and a realization of (63) is given by (64) and (65).

The data are sampled with sample period  $T_s = 1$  s. Let  $u_{\min} = -2$ ,  $u_{\max} = 2$ ,  $\Delta u_{\min} = -1$ ,  $\Delta u_{\max} = 1$ ,  $\ell = 20$ ,  $\bar{Q} = 10I_{\ell-1}$ ,  $\bar{P} = 20$ ,  $R = I_\ell$ ,  $P_0 = 10^3 I_{2\hat{n}}$ , and  $\theta_0 = [0_{1 \times (2\hat{n}-1)} \ 1]^T$ . The initial plant (77) is initialized with  $x(0) = [2.5 \ -1.4]^T$ , and the modified plant (63) is initialized with  $x(0) = [-0.039 \ 1.508 \ 0 \ 0]^T$ . The output constraint is given by (5), where  $C = [1 \ -1]^T$ , and  $\mathcal{D} = [-20 \ -20]^T$ . For this example, PCAC uses (41)–(45) with

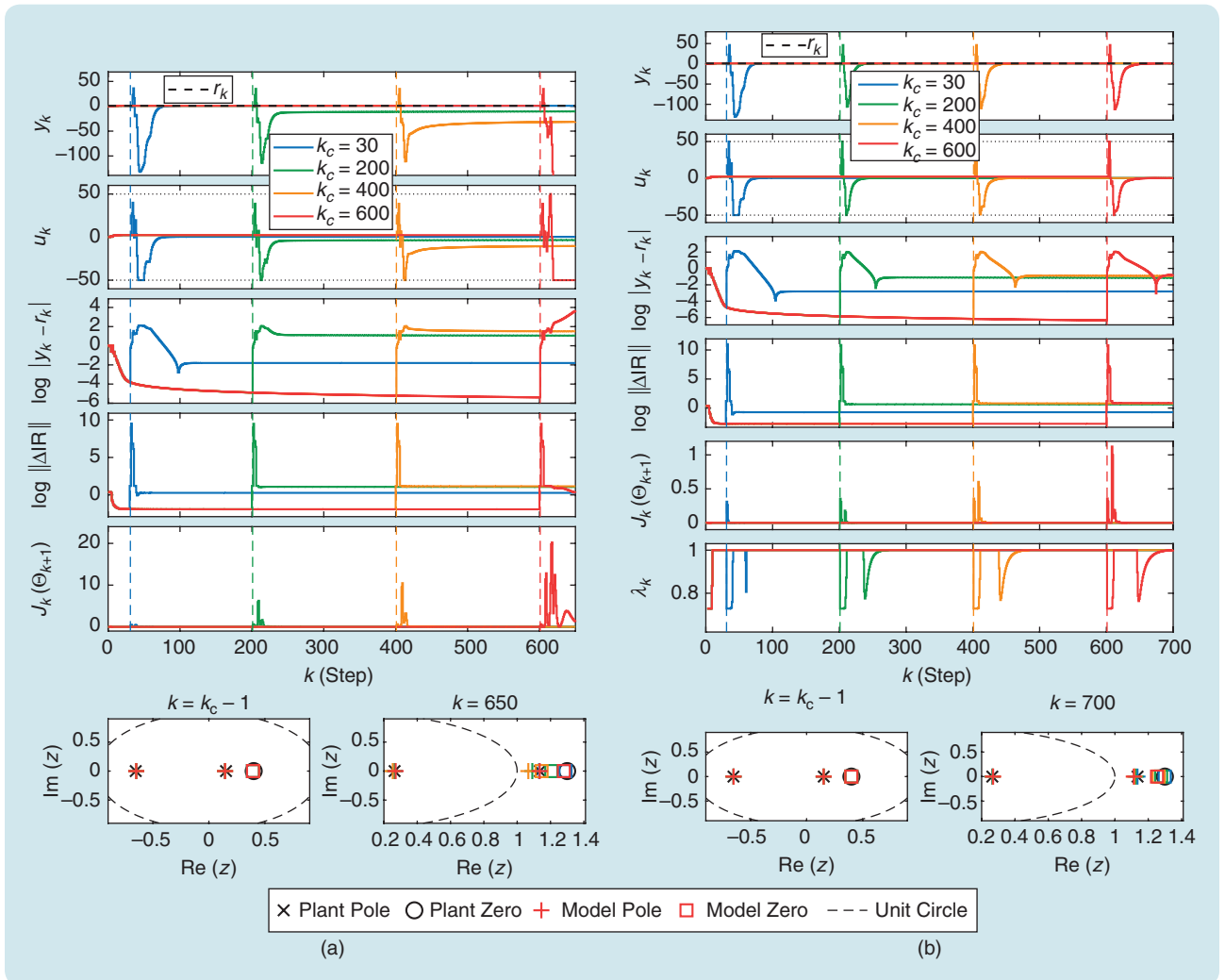


**FIGURE 20** Example 8: Command following with dynamics that abruptly change at step  $k_c$  represented by the dashed vertical line for  $r_k \equiv 1$  and various values of  $k_c$ . At step  $k_c$ , the discrete-time asymptotically stable minimum-phase single-input, single-output plant (46) changes to the discrete-time unstable nonminimum-phase plant (53). (a) Constant-rate forgetting with  $\lambda = 1$ . Note that, as for larger values of  $k_c$ , the command-following error after the change is larger. In particular, for  $k_c = 600$ , the slow reidentification after the abrupt change causes the control input to saturate and the output error to diverge. Note that the maximum value of the recursive least squares (RLS) cost  $J_k(\theta_{k+1})$  (12) increases as  $k_c$  increases. This is due to the fact that  $\lambda = 1$ , and, thus, RLS does not discount data from before the abrupt change. The two bottom-most plots compare the poles and zeros of the identified model with the poles and zeros of the plant at  $k = k_c - 1$  and  $k = 650$ . (b) Variable-rate forgetting (VRF) (21) with  $\eta = 0.9$ ,  $\tau_n = 5$ , and  $\tau_d = 10$ . In contrast with (a), for each  $k_c$ ,  $y_k$  approaches the command after the abrupt change. The sixth plot from the top shows that the VRF factor  $\lambda_k$  is activated near  $k_c$ .  $\Delta IR$ : the  $L_2$ -norm difference between the 30-step impulse response of the plant and model.

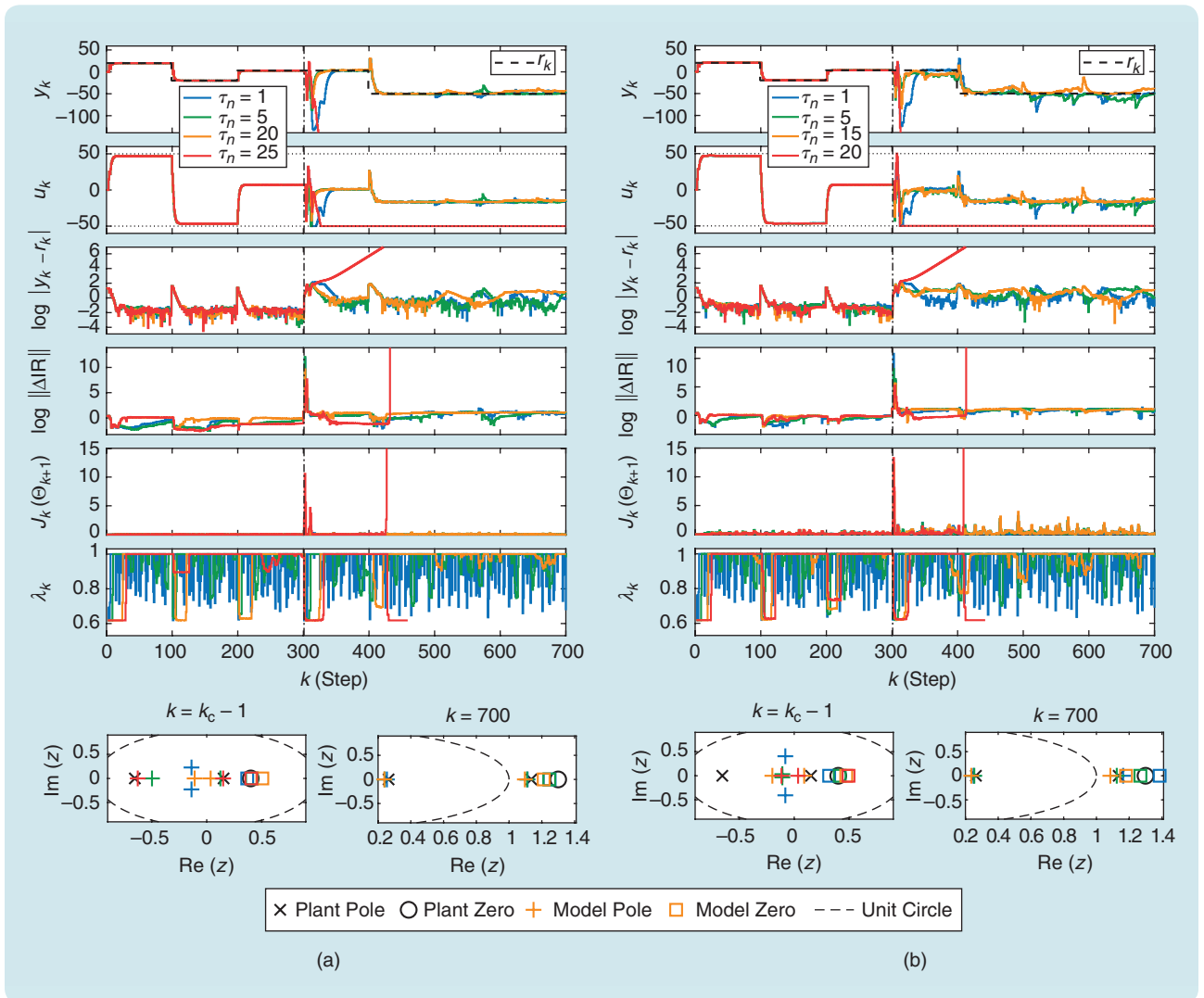
$S = 10^6 I_2$ . A strictly proper model is used for identification in PCAC. Figure 22 shows the response of PCAC for two different levels of sensor noise and various values of  $\hat{n}$  using the command profile (76) and VRF (21) with  $\eta = 0.5$ ,  $\tau_n = 25$ , and  $\tau_d = 125$ .

Figure 22 shows that, for a plant that abruptly transitions from (77) to (63) with  $\zeta = 0.01$ , output transients and constraint violations occur after the abrupt transition. However, as the identification accuracy improves, the output transients dissipate, and the constraints are satisfied asymptotically. Additionally, note that overparameteriza-

tion of the model facilitates identification and, thus, constraint enforcement.  $\diamond$

## CONCLUSIONS

This article presented a numerical investigation of PCAC, which uses closed-loop identification to identify a model for constrained receding-horizon control optimization. The identified model uses an input-output structure with BOCF realization, which enables output-feedback control without the need for an observer. PCAC was applied to 10 numerical examples that demonstrate command following and disturbance



**FIGURE 21** Example 9: Command following with dynamics that abruptly change from (46) to (53) at step  $k_c = 300$  with sensor noise. Predictive cost adaptive control uses the command profile (76) and variable-rate forgetting (VRF) (21) with  $\eta = 0.5$ ,  $\tau_d = 5\tau_n$ , and various values of  $\tau_n$ . (a) The sensor noise  $v_k$  is a zero-mean, Gaussian white noise sequence with a standard deviation of 0.1. Note that, before the abrupt change and for all values of  $\tau_n$ ,  $y_k$  approaches each step command. After the abrupt change, however,  $y_k$  approaches the command for  $\tau_n = 1$ ,  $\tau_n = 5$ , and  $\tau_n = 20$ , and it diverges for  $\tau_n = 25$ . Furthermore, for  $\tau_n = 25$ , the impulse-response error and recursive least squares (RLS) cost diverge approximately at  $k = 430$ . Note that, as  $\tau_n$  increases, the VRF factor  $\lambda_k$  becomes less sensitive to sensor noise and is activated only at the abrupt change and at each step-command change. (b) The sensor noise  $v_k$  is a zero-mean, Gaussian white noise sequence with a standard deviation of 0.3. Note that, compared to (a), since the sensor-noise level is larger, the value of  $\tau_n$  for which the output, impulse-response error, and RLS cost diverge is lower; namely,  $\tau_n = 20$ .  $\Delta IR$ : the  $L_2$ -norm difference between the 30-step impulse response of the plant and model.

rejection subject to state and control constraints. Based on these examples, “Guidelines for Selecting Hyperparameters” presents guidelines for selecting hyperparameters.

The performance of PCAC was investigated numerically to highlight the interplay between closed-loop identification and control. Three issues were considered, namely, persistency, consistency, and exigency. Persistency is needed for the unambiguous estimation of model parameters; consistency ensures that the parameter estimates are asymptotically unbiased; and exigency prioritizes the identification of model features that are essential for achieving the control objective. When the persistency of the commands and disturbances is not sufficient for identification, PCAC was shown to provide additional self-generated persistency through the control input.

Since the control input produced by PCAC is correlated with the disturbance and sensor noise, the parameter estimates obtained from closed-loop identification based on RLS are not

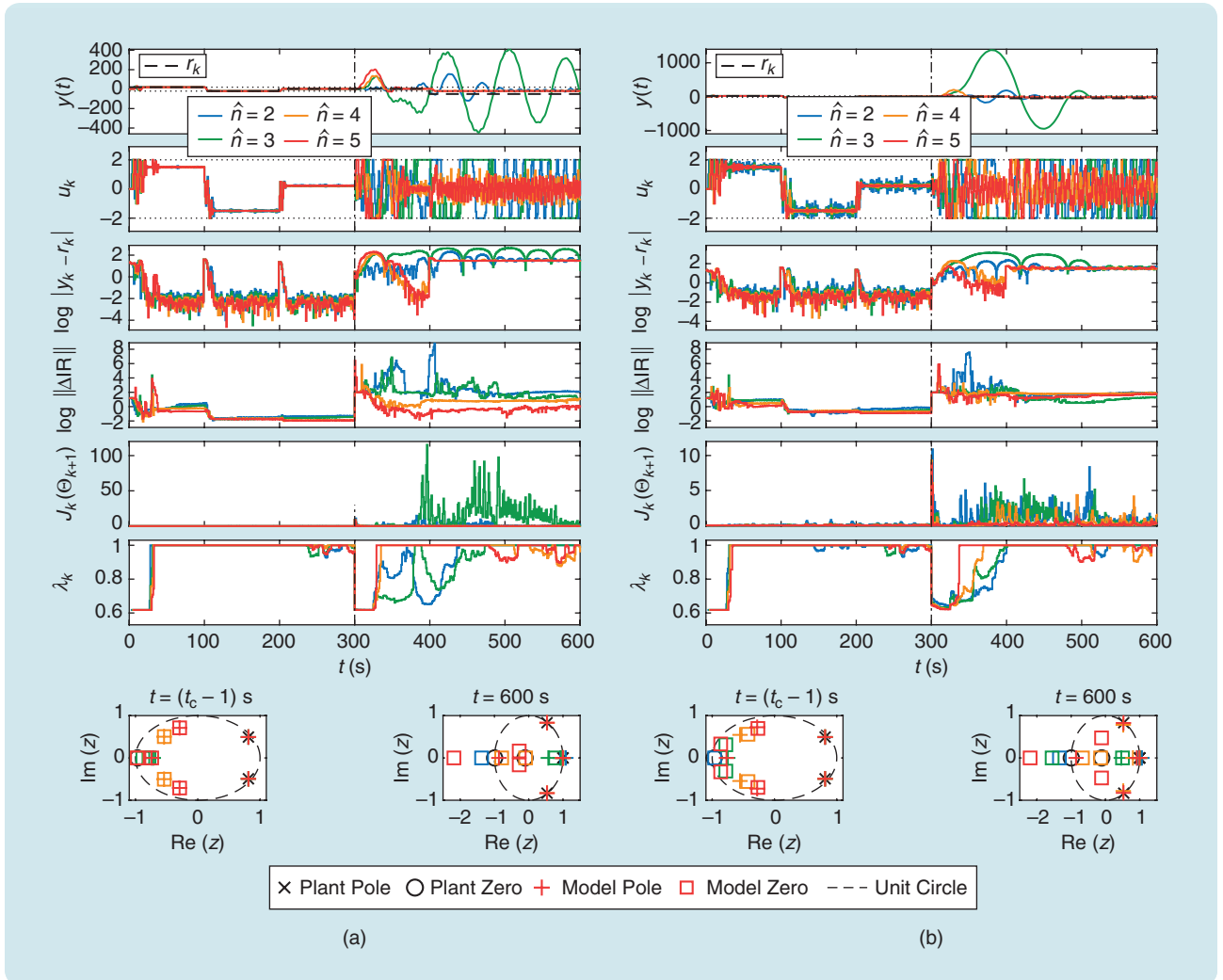


**FIGURE 22** Example 10: Command following with dynamics that abruptly change from (77) to (63) at 300 s with sensor noise and an output constraint for various values of  $\hat{n}$ . Predictive cost adaptive control uses the command profile (76) and variable-rate forgetting (21) with  $\eta = 0.5$ ,  $\tau_n = 25$ , and  $\tau_d = 125$ . (a) The sensor noise  $v_k$  is a zero-mean, Gaussian white noise sequence with a standard deviation of 0.01. Note that, before the abrupt change occurs and for each value of  $\hat{n}$ ,  $y(t)$  approaches the step commands, and the output constraint is satisfied at all times. In the underparameterized cases  $\hat{n} < n = 4$ , after the abrupt change occurs, the double integrator and lightly damped poles are poorly identified by recursive least squares (RLS), causing  $y(t)$  to oscillate and violate the constraint until the end of the simulation. In contrast, in the exact and overparameterized cases  $\hat{n} \geq n = 4$ , after the abrupt change occurs,  $y(t)$  only temporarily violates the constraint during reidentification. Additionally, after  $t = 338$  s,  $y(t)$  is more damped than the underparameterized cases, and the output constraint is enforced at all times. Note that the last segment of  $y(t)$  is infeasible. (b) The sensor noise  $v_k$  is a zero-mean, Gaussian white noise sequence with a standard deviation of 0.1. Note that, due to the higher sensor-noise level, the oscillation amplitude and output-constraint violation for  $\hat{n} < n = 4$  are more pronounced in (b) than in (a). Furthermore, note that, in both (a) and (b), for  $\hat{n} = 2$ , RLS is able to capture the two integrators of the plant, whereas, for  $\hat{n} = 3$ , the three poles of the model are unable to capture the two integrators and two undamped poles of the plant, causing the identification and transient response to be poorer.  $\Delta IR$ : the  $L_2$ -norm difference between the 30-step impulse response of the plant and model.

consistent and, thus, are asymptotically biased. Although the bias was shown to degrade the accuracy of PCAC, this effect was mitigated to some extent by using RLS with VRF. PEM and IV were considered as alternatives to RLS/VRF. Although PEM and IV are more accurate than RLS/VRF for both open- and closed-loop identification, these methods were found to be less compatible with PCAC than RLS/VRF.

Finally, the interplay between control and identification was further examined in terms of exigency, which is the ability of the closed-loop identification to prioritize the model features needed to achieve the control objective. Numerical examples, such as the estimation of the plant dc gain for set-point command following, showed that exigency is manifested in the continuing refinement of the identified model.

The numerical examples in this article were designed to expose features of PCAC that motivate the investigation of stability and performance guarantees. A major next step is to extend the method to various classes of nonlinear systems [74]. Finally, the performance of PCAC on linear and nonlinear numerical examples provides further motivation to apply this technique to physical examples.

## ACKNOWLEDGMENTS

We thank Nima Mohseni, Adam Bruce, and the reviewers for numerous helpful comments and suggestions. This research was supported by the U.S. Office of Naval Research under BRC grant N00014-18-1-2211.

## AUTHOR INFORMATION

**Tam W. Nguyen** received the M.Sc. degree in mechatronics engineering and the Ph.D. degree in control systems from the Free University of Brussels, Belgium. He then served as a postdoctoral researcher in the Aerospace Engineering Department at the University of Michigan, Ann Arbor. He is currently an assistant professor in the Department of Electrical and Electronics Engineering at the University of Toyama, Toyama, Japan. His research interests include constrained control for aerial-robotics applications.

**Syed Aseem Ul Islam** received the B.Sc. degree in aerospace engineering from the Institute of Space Technology, Islamabad, and the Ph.D. degree in flight dynamics and control from the University of Michigan, Ann Arbor, Michigan, USA. He is currently a research fellow at the University of Michigan, Ann Arbor, Michigan, USA. His research interests include data-driven adaptive control for aerospace applications.

**Dennis S. Bernstein** received the Sc.B. degree from Brown University and the Ph.D. degree from the University of Michigan in Ann Arbor, Michigan. He is currently a professor in the Aerospace Engineering Department, University of Michigan, Ann Arbor, Michigan, USA. His research interests include identification, estimation, and control for aerospace applications. He is the author of *Scalar, Vector, and Matrix Mathematics*, published by Princeton University Press.

**Ilya V. Kolmanovskiy** (ilya@umich.edu) is a professor in the Department of Aerospace Engineering at the University of

Michigan, Ann Arbor, Michigan, USA. His research interests include control theory for systems with state and control constraints as well as control applications for aerospace and automotive systems. He received the Ph.D. degree from the University of Michigan in 1995. He is a Fellow of IEEE and is named as an inventor on more than 100 U.S. patents.

## REFERENCES

- [1] W. Kwon and S. Han, *Receding Horizon Control: Model Predictive Control for State Models*. Berlin: Springer-Verlag, 2006.
- [2] S. Di Cairano and I. V. Kolmanovskiy, "Real-time optimization and model predictive control for aerospace and automotive applications," in *Proc. Amer. Contr. Conf.*, 2018, pp. 2392–2409. doi: 10.23919/ACC.2018.8431585.
- [3] U. Eren, A. Prach, B. B. Koçer, S. V. Rakovic, E. Kayacan, and B. A. Açikmes, "Model predictive control in aerospace systems: Current state and opportunities," *J. Guidance, Control, Dynamics*, vol. 40, no. 7, pp. 1541–1566, 2017. doi: 10.2514/1.G002507.
- [4] T. Samad et al., "Industry engagement with control research: Perspective and messages," *Ann. Rev. Contr.*, vol. 49, pp. 1–14, 2020. doi: 10.1016/j.jarcontrol.2020.03.002.
- [5] S. Boyd and L. Vandenberghe, *Convex Optimization*. Cambridge, U.K.: Cambridge Univ. Press, 2004. doi: 10.1017/CBO9780511804441.
- [6] S. S. Keerthi and E. G. Gilbert, "Optimal infinite-horizon feedback laws for a general class of constrained discrete-time systems: Stability and moving-horizon approximations," *J. Optim. Theory Appl.*, vol. 57, no. 2, pp. 265–293, 1988. doi: 10.1007/BF00938540.
- [7] E. F. Camacho and C. Bordons, *Model Predictive Control*, 2nd ed. Berlin: Springer-Verlag, 2007.
- [8] J. B. Rawlings, D. Q. Mayne, and M. M. Diehl, *Model Predictive Control: Theory, Computation, and Design*, 2nd ed. Nob Hill Publishing, LLC, 2017.
- [9] S. V. Rakovic and W. S. Levine, *Handbook of Model Predictive Control*. Birkhäuser, 2019.
- [10] K. Fruzzetti, A. Palazoglu, and K. McDonald, "Nonlinear model predictive control using Hammerstein models," *J. Process Control*, vol. 7, no. 1, pp. 31–41, 1997. doi: 10.1016/S0959-1524(97)80001-B.
- [11] H. H. J. Bloemen, T. J. Van Den Boom, and H. B. Verbruggen, "Model-based predictive control for Hammerstein–Wiener systems," *Int. J. Control*, vol. 74, no. 5, pp. 482–495, 2001. doi: 10.1080/00207170010014061.
- [12] J. Zhang, K.-S. Chin, and M. Lawryn'czuk, "Nonlinear model predictive control based on piecewise linear Hammerstein models," *Nonlinear Dynam.*, vol. 92, no. 3, pp. 1001–1021, 2018. doi: 10.1007/s11071-018-4105-5.
- [13] T. Hu and Z. Lin, *Control Systems With Actuator Saturation: Analysis and Design*. Birkhäuser, 2001. doi: 10.1007/978-1-4612-0205-9.
- [14] S. Tarbouriech, G. Garcia, J. M. G. da Silva, and I. Queinnec, *Stability and Stabilization of Linear Systems With Saturating Actuators*. Berlin: Springer-Verlag, 2011. doi: 10.1007/978-0-85729-941-3.
- [15] D. S. Bernstein and A. N. Michel, "A chronological bibliography on saturating actuators," *Int. J. Robust Nonlinear Control*, vol. 5, no. 5, pp. 375–380, doi: 10.1002/rnc.4590050502.
- [16] D. Limón, I. Alvarado, T. Alamo, and E. F. Camacho, "MPC for tracking piecewise constant references for constrained linear systems," *Automatica*, vol. 44, no. 9, pp. 2382–2387, 2008. doi: 10.1016/j.automatica.2008.01.023.
- [17] G. C. Goodwin, D. S. Carrasco, D. Q. Mayne, M. E. Salgado, and M. M. Serón, "Preview and feedforward in model predictive control: Conceptual and design issues," *IFAC Proc. Volumes*, vol. 44, no. 1, pp. 5555–5560, 2011. doi: 10.3182/20110828-6-IT-1002.02298.
- [18] S. M. Kuo and D. Morgan, *Active Noise Control Systems: Algorithms and DSP Implementations*. Hoboken, NJ: Wiley, 1995.
- [19] L. Grüne and J. Pannek, *Nonlinear Model Predictive Control*. Berlin: Springer-Verlag, 2017, pp. 45–99.
- [20] N. L. Ricker, "Model predictive control with state estimation," *Ind. engineering chemistry Res.*, vol. 29, no. 3, pp. 374–382, 1990. doi: 10.1021/ie00099a013.
- [21] A. Wills, D. Bates, A. Fleming, B. Ninness, and R. Moheimani, "Application of MPC to an active structure using sampling rates up to 25kHz," in *Proc. Conf. Dec. Contr.*, 2005, pp. 3176–3181. doi: 10.1109/CDC.2005.1582650.
- [22] I. V. Kolmanovskiy and V. Winstead, "A receding horizon optimal control approach to active state and parameter estimation in automotive systems," in *Proc. IEEE Int. Conf. Control Appl.*, 2006, pp. 2796–2801.
- [23] K. Zhang and Y. Shi, "Adaptive model predictive control for a class of constrained linear systems with parametric uncertainties," *Automatica*, vol. 117, p. 108974, 2020. doi: 10.1016/j.automatica.2020.108977.

